Optically Obscured Quasars

Frank J. Masci

Fourth Year Project

School of Physics, The University of Melbourne

Supervisor: Dr R. Webster

Submitted: 12th November, 1993

I authorize the Chairman of the School of Physics to make or have a copy of this report for supply to any person judged to have an acceptable reason for access to the information, i.e., for research, study or instruction.

Signed:.....

This is not the end.
It is not even the beginning of the end.
But it is, perhaps, the end of the beginning.

WINSTON CHURCHILL

Abstract

The Parkes catalogue of flat spectrum radio sources has a significant number of objects identified as compact radio emitters which fail to coincide with an optical image. Sources identified in the radio alone are classified as empty fields; however from the statistical distribution of successful identifications in the radio, most of these sources are quasars. It is likely that many of these sources have been missed in the optical because they are exceedingly red in color, thus we will test the hypothesis that some of these optically faint objects are bright in the infrared (IR). Quasars at large redshifts may be severely obscured (and reddened) due to intervening dust either within or between other galaxies.

The best test for this hypothesis will come from imaging the empty fields in the infrared. Observations at infrared wavelengths were made at the AAT in June and if a bright IR source was found at the location of the radio source, an IR spectrum was taken and an identification made. A comparison of the spectra of such sources with the spectra of unreddened sources are made to determine whether the IR emission mechanism is due to the presence of dust. Otherwise the extreme reddening may be attributed to a totally intrinsic phenomenon.

Contents

1 Introduction

1.1 What is a Quasar?

Quasars have been a remarkable observational discovery. These objects appear only as faint starlike images on photographic plates and CCDs[1] and yet they are emitting enormous quantities of energy from radio to γ-ray wavelengths. These are the only objects seen in large Numbers at sizeable redshifts. The furthest quasars detected are receeding at speeds of 90-95% of the speed of light, this corresponds to distances of greater than 10 billion light years[2]. Such large distances indicate that we are observing these objects as they appeared in the early stages of the universe. Quasars remain among the most puzzling of all celestial objects. If quasars are at the cosmic distance implied by their redshifts, they must be extremely luminous objects, some may be emitting 10^{13} times more power than the sun. A galaxy such as our own at the distance of a quasar some 10 billion light years away would appear at least ten magnitudes fainter, which means that the quasar would be intrinsically 10^4 times brighter.

The first optically identified radio source was made by T.Matthews and A.Sandage in 1960, it was a 16th magnitude starlike object at the position of the radio object 3C48 (3C means third Cambridge catalog, compiled by Martin Ryle during the 1950s at Cambridge). The spectrum of 3C48 had broad emission lines that could not be identified and it emitted more ultraviolet light than an ordinary main sequence star.

The term "Quasar", short for "Quasi-stellar object (QSO)", was originally applied only to the starlike counterparts of certain strong radio sources whose optical spectra exhibit redshifts much larger than those of galaxies. Before long, however, a class of quasi stellar objects was discovered with large redshifts that have little or no emission at radio wavelengths. "Quasar" is now commonly applied to starlike objects with large redshifts exhibiting certain spectral properties (which will be discussed later), regardless of their radio flux output.

[1] Charge coupled devices-electronic chips which convert an incident light intensity to some measurable current.

[2] Assuming a cosmology with parameters $q_o = 0.5$ and $H_o = 50 km/sec.Mpc$.

Current estimates of quasar redshifts range almost all the way up to 5, the first and smallest measured being 0.158 (Schmidt 1965) (see figure 3). The largest recorded redshift to date is 4.9, which corresponds to a recessional velocity approaching $0.95c$ (Schneider et al.1991). Normal galaxies on the other hand, that can be classified according to their structural features (ie spirals, ellipticals etc.) where their light is mostly dominated by stars can exhibit redshifts as great as 0.3. Redshift is defined as

$$z = \frac{\lambda - \lambda_o}{\lambda_o}$$

where λ_o is a wavelength in the rest frame of the object which is measured as a larger wavelength λ for a receeding source in the observer's frame. Thus every wavelength λ_o in the object's frame is shifted by a factor of 1+z when measured on Earth. Put another way, the quantity 1+z expresses how much the universe has expanded between the emission of a photon and its observation. In some quasar spectra the Lyman α emission line from neutral hydrogen which is normally in the UV at 1216Åis shifted into the visible part of the spectrum (observed at 4000Å-blue region for $z \sim 2.3$). This strong emission line (see figure 12) is often the most conspicuous feature in all quasar spectra. The relation relating the redshift z of an object to its velocity of recession, given that it is receeding at a relativistic speed is given by

$$v = \left[\frac{(1+z)^2 - 1}{(1+z)^2 + 1}\right] c$$

(where c is the speed of light). This relation follows directly from the relativistic Doppler shift formula, stating that the shift in freqency in some wave between that emitted by a source and detected by an observer is due to the relative velocity between them. For low velocities ($v \leq 0.1c$) the relation becomes $v = zc$.

Distances to quasars are inferred by the use of the "Hubble law", which states that the velocity of recession v of some distant object is proportional to its distance d from us, or more precisely it states that the redshift increases linearly with distance. The Hubble law can be written as

$$v = Hd$$

The constant of proportionality H is called Hubble's constant, measured to within a factor of two, its value is estimated to be between 50-100km/s.Mpc.

Thus given that the redshift z is cosmological in origin (ie being due to the expansion of the universe) the corresponding distance to the object can be easily found, but only precisely to within a factor of two. This method holds particularly well for highly redshifted sources.

It is the spectrum taken of a suspected quasar that will settle the question of its identification. An apparent feature is the presence of broad emission or absorption lines in the optical (see figure 4) which are all greatly shifted to the red and the presence of an excess of UV flux which may be intrinsically greater than 10^5 times the sun's UV light output. Despite many of the techniques for undertaking quasar surveys today, such as X-ray, infrared and radio surveys, the great majority of quasars have been discovered optically.

Quasars have been identified on the basis of their UBV colors by examining photographs of "blue" stellar objects or objects showing an ultraviolet excess. The UBV color system refers to apparent magnitudes in the ultraviolet, blue and visual bands of the spectrum centered about 3600Å, 4400$\mathring{A}$ and 5500$\mathring{A}$ respectively. Color indices are defined by the quantities $U-B$, $B-V$ and are based on the star Vega having $U-B=B-V=0$. The distinction of quasars is therefore that they have a relatively large-negative $U-B$ or $B-V$ value. It is never possible on the basis of the UBV colors alone to be positive that a candidate is a quasar without an actual spectrum. Hot stars such as white dwarfs also tend to show an ultraviolet excess, but they are ruled out once a spectrum is taken and a redshift measured.

Initially, quasars were found with radio telescopes or interferometers. It was Ryle and Sandage in 1964 who first conceived the idea of using ultraviolet strength as a clue in searching for optical counterparts of the identified radio sources. It was noted by Sandage that objects with excess UV emission were more plentiful than known radio sources in a typical stellar field. He discovered that some of these high UV emitters exhibited redshifts that qualify them as quasars even though no radio emission was detected from them. Observations have shown that only a small fraction of identified quasars ($\approx$ 2%-Peacock & Dunlop 1985) are strong radio emitters (radio loud) and the rest are termed "radio quiet" (see figure 1). Thus virtually all quasars discoverable optically today are rarely strong radio sources. Most radio emission from sources is seen to be emitted from extended lobes at a great distance from the nucleus as in other active galaxies. As radio surveys were done at progressively shorter wavelengths, more compact unresolved sources were seen, which were able to be identified optically as quasar cores (Wall

1983). These quasar cores are also termed "flat" spectrum radio sources.

Throughout the many optical surveys based on color, several thousand quasars have now been identified. Most have been identified in the redshift range $1 \leq z \leq 2.5$. Note that only quasars with redshifts below 2 can be clearly identified by their optical colors alone as being blue stellar objects. For redshifts much above 2, a redshift bias is introduced. The strong Ly-α line in the UV in which most of the UV flux resides can be shifted into the optical, thereby reddening the $U - B$ color so that identification based on UV excess may become very inefficient. This redshift bias can be overcome by identifying the high redshift quasars by their redshifted emission lines by taking highly resolved spectra (Smith 1981). The lines remaining the most prominent out to $z \sim 2.5$ are Ly-α (1216Å) and C IV (1550Å). Identifications based on spectra alone can lead to more complete samples at a larger range of redshifts than the color surveys.

If it was possible to conduct an instantaneous survey of the universe, then one might find that there should be at least 10^6 quasars in existence today. Numbers from optical surveys have been compared and assembled (Braccesi 1983) and findings show that to a B-magnitude of 21 there appear to be about 40 quasars per square degree, which corresponds to somewhat over a million over the whole sky. The problem has been in identifying quasar samples within well defined redshift ranges, especially at high redshifts where optical surveys appear to be incomplete. Observations have shown that there tends to be a dramatic redshift cutoff of quasars for $z > 2.22$ (Véron 1983), in particular only 20 are known with $z > 4$. This may be due to some type of unknown quasar evolution. Such results are quite different from the numbers of quasars expected from current evolutionary models based on luminosity (Weedman 1986). They predict that $\sim 41\%$ of quasars to magnitude 22 are expected to be within the interval $2.5 < z < 5$ (see table 1). It appears that some bias may be present within the optical surveys which may hide a population of very high redshift quasars. Current efforts are being made to search for quasars at other wavelengths (X-ray & infrared) in order to understand their true distribution.

The light output of some quasars has been observed to change significantly in a matter of days (Valtaoja 1985). This tells us that some variable component of the quasar, if not the entire quasar, may be at least as small

Quasar redshift distributions for optical surveys

Optical limit (B mag)	Number deg^{-2} $z<2.0$	Number deg^{-2} $2.0\leqslant z<2.5$	Number deg^{-2} $2.5\leqslant z\leqslant 5.0$	Most probable z
16	6.2×10^{-3}	0.3×10^{-3}	0.3×10^{-3}	<0.1
19	2.5	0.24	0.37	0.3
22	140	41	124	1.5
25	950	340	1340	1.9
28	3550	1440	6200	2.2

Table 1: Anticipated redshift distribution of quasars (number per square degree) up to various magnitude limits, also shown is the most probable redshift at which numbers are expected to peak (Weedman 1986).

as our solar system[3]. The major problems that quasars pose, is how to interpret the power radiated, $\sim 10^{40}$W, and how to generate it from such a small region. If they were much closer then the power that needed to be explained would of been correspondingly less. The physical conditions in such a small region may be unlike those found anywhere else in the universe, the generally favoured model is that the power source may be from the direct conversion of matter into energy due to the presence of a black hole. The observation of quasars at new wavebands (most recently in the far-infrared, X-rays, γ-rays) has continued to shed light on the nature of their possible energy processes.

1.2 The Energy Continuum.

Quasars emit their energy at a large range of wavelengths, from the radio through to the γ-rays, with some quasars showing appreciable amounts being emitted in the radio, infrared, UV and/or γ-ray regions. The continuum emission contributing to the quasar spectrum extends from 10^8(radio) to 10^{26}Hz(γ-rays) (see figure 1). Most quasars cannot be seen equally as well at all wavelengths, though the majority show strikingly similar features and behaviour throughout the UV-optical-IR region. Unlike stellar blackbody (thermal) spectra[4], the spectral energy distribution can be well approximated by a power law:

$$F(\nu) = F_o\nu^{-\alpha}$$

[3]Variation on a time scale Δt implies that the source is no larger than about $c\Delta t$.

[4]Radiation from stars can be well approximated by the Planck radiation distribution law.

where $F(\nu)$ is the emitted flux at some freqency ν and α is defined as the spectral index. On a log-log plot of the spectrum we have

$$logF(\nu) = -\alpha log\nu + constant$$

so that the spectral index α is simply the slope. Throughout a typical quasar spectrum, α often takes the values $0 \leq \alpha \leq 1.5$ being more uniform in certain regions than others, whereby then the emission is believed to be nonthermal in origin as will be shortly discussed. A typical quasar spectrum is taken to be a composite of power laws with average slopes α: 1 from 5000Å(optical) to 200μ (far-IR), 0.5 from 5000Åto 1000Å(UV), 1.3 from 1000Åto 10Å(X-rays) and 0.7 from 10Å(1.2keV) to 0.12Å(100keV-γ-ray region). Furthermore the range of slopes observed in the radio leads us to define two distinct categories for quasars based on the spectral index α: flat and steep spectrum radio sources, with the division at $\alpha \approx 0.5$ (see figure 1). It is often more convenient to use $\nu F(\nu)$ rather than $F(\nu)$ to represent the spectra because $\nu F(\nu)$ is a measure of the energy emitted per unit logν so that the total luminosity emitted is the integrated area under the spectrum. Thus, as well as for scaling reasons it is normally useful to plot $\log(\nu F_\nu)$ versus logν as in figure 1. From these plots it can be seen at which frequencies the energy output peaks.

The majority of the continuous emission seen in different components of the quasar spectrum has been modeled accordingly to different radiation mechanisms-usually physically unrelated. Emission is mostly believed to arise from either a thermal or non-thermal process or a combination of the two (Impey 1992). In turn, each process has been modeled according to a region in the quasar from which the type of radiation is believed to be emitted from giving us information on the nature of that region such as temperature (Blanford 1990). Thermal processes are generally associated with atomic energy levels being excited by collisional processes among particles moving non-relativistically with a corresponding temperature of $\sim 10^4$K. The thermal radiation arising from this process is believed to be from dense optically thick gases and emerges as a thermal blackbody spectrum having an associated effective temperature T. The infrared emission is believed to be due to such thermal processes-possibly emission by dust heated by some higher frequency radiation (Sanders et al. 1989). Most of the infrared flux peaks in a region called the "infrared bump" situated in the range $10^{12} - 10^{14.2}$Hz

(see fig.1). The emission lines in the optical, providing information on velocities, temperatures, densities and redshifts may represent the re-radiation of energy by individual ions, again derived from some initial continuum source.

Non-thermal radiation, can arise from particles moving at relativistic velocities-their energy distribution may directly reflect the initial energy source powering the quasar (Blandford 1990). This radiation is not due to collisional processes. The best known form of non-thermal emission is from synchrotron processes-where radiation is produced by the gyrating motion of relativistic electrons in a magnetic field. This type of emission is used to account for most of the radio and UV flux aswell as some of the X-ray and optical emission. Any region of the quasar spectrum which appears to have a uniform shape according to $F_\nu \propto \nu^{-\alpha}$ is often attributed to some non-thermal mechanism, since non-thermal sources are usually characterised by an output radiation spectrum that is a perfect power law (Jones et al.1974). Note that non-thermal radiation may in some cases be considerably reprocessed or absorbed by gas clouds thereby contributing as a thermal spectrum. Some of the thermal energy may also be transformed by being boosted to higher freqency non thermal radiation, this can occur by radiation being compton scattered off relativistic particles into our line of sight. The "Hard" radiation (γ-rays & X-rays) is believed to some extent arise from such boosting of lower frequency radiation (Kardashev et al.1985). These interfering mechanisms make the analysis of quasar spectra exceedingly difficult. It is uncertain which and to what extent each process contributes to lead to what is observed in each waveband.

It is believed that different mechanisms operating on different scales could contribute to the optical, UV and X-ray emission (Rees 1985) due to the sharp changes in spectral indices connecting these regions. There appears to be a strong departure from a power law in the optical-UV region (10^{15}-10^{16}Hz), a feature most commonly referred to as "The big blue bump". It is believed to be from a thermal continuum emitted from a "hot accretion disk" (Malkan 1983)-a necessary part of any quasar model involving black holes. There has been a major difficulty with the UV - X-ray continuum, this radiation is known to suffer heavy absorption and extinction by the intervening medium which is mostly composed of matter made up of heavy elements. In particular the matter in our own galaxy obscurs most of the radiation in these wavebands. These effects need to be untangled from the spectrum before we can proceed to study the quasar. Both thermal and

nonthermal processes are believed to be present at a non-neglible level in all quasars, the major problem has been in explaining the departure of a quasar spectrum from a power law continuum. In particular the observed variation in spectral indices between different wavebands has been difficult to account for. The aim is to isolate those parts of the spectrum that can be used to understand the primary luminosity generation.

It has been argued (Blandford & Rees 1978) that the radiation emitted by a quasar may not be necessarily isotropic but may be beamed in certain directions-sometimes towards us. Such anisotropic emission can arise from particals radiating from a cloud or some quasar plasma which moves at a relativistic velocity. In some cases the radiation produced from such a cloud may be concentrated in a cone projected towards us or nearly so. As a result we may see an enhanced luminosity from the source. Generally luminosities are determined from the continuous spectrum emitted by a source, this assumes that the flux is emitted isotropically and not directionally dependent, though this assumption may not be always correct. Radiation may be relativistically beamed from some quasars. Evidence for such is provided by the observed superluminal motions in the radio jets (see section 1.3) of some sources (Cohen *etal.* 1983). A class of quasars believed to emit beamed radiation are the "Blazars" (Angel & Stockman 1980), among which are classified the optically violently variables (OVVs) which show rapidly varying emission lines and BL-Lacertae objects with no emission lines and a very uniform spectral energy distribution. The variability in the light output of these objects is consistent with models of synchrotron emitting plasmas moving relativistically (Huchra 1977)-hence showing that beamed radiation is mostly non-thermal in origin as expected. The blazars represent $\sim 1\%$ of total quasars known (Maccacaro *etal.* 1984).

1.3 Quasar models.

Quasars tend to show similar properties to other types of active galactic nuclei (AGN), all classified on the basis of their spectral properties and appearence, and all of which emit large amounts of non-thermal energy-the blazars, radio galaxies and Seyfert galaxies being some of them. The Seyfert galaxies (Carl Seyfert 1943) in particular are believed by many to be the low-power analogs of the quasars. They exhibit a quasar-like core embedded

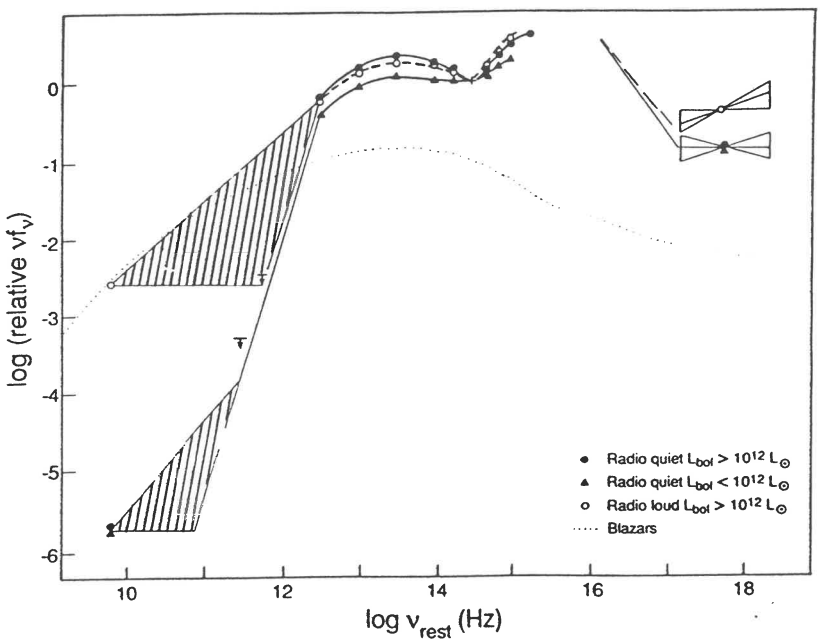

Figure 1: A *log-log* plot of an average quasar spectrum from the radio (10^{10}Hz) to the $\gamma-$ray region (10^{18}Hz) showing the change in α. The data points are mean values for quasars from the Palomar Green sample (Green *etal.* 1986). The hatched regions represent the range of spectral indices observed in the radio (higher region-radio louds, lower-radio quiets). Also shown (dotted line) is the energy distribution for blazars-Impey (1988) (Sanders et al.1989).

in a visible spiral galaxy and have modest redshifts from 0.02 to 0.8. Some quasars have also been seen to sit in a "host" galaxy. Evidence is provided from the deep imaging of quasars with $z < 0.5$, which appear to be surrounded by some extended nebulosity (Gehren et al.1984). Malkan (1984) has also shown that some of these images appear to be consistent with spiral galaxies. The seyferts show very similar emission spectra as the quasars and it may be that the physical conditions in the regions providing the spectra may be the same. Nearby AGN seem to be a natural starting point to model the structure of quasars even though their luminosites may differ by as much as a factor of 10^7.

The distinction of all quasars with other AGN is their extreme "compactness" and their ability to generate extraordinary luminosities within small volumes. This luminosity generation has been accounted for in many ways. The luminosity of a typical quasar is of order $10^{12}L_\odot$[5], far too large for its source to be a star, since the most massive stars are of order $10^2M_\odot$ with corresponding energy outputs of about $10^5L_\odot$. It is possible to put together enough stars to reach a quasar luminosity, but this has been generally rejected on the basis of variability studies, which show that the light intensity from a quasar is seen to vary from days to years, implying that the emitting regions are no larger than one light year. It is not possible for such a region to contain enough stars needed to account for energy generation by nuclear fusion. It is expected that the large energies released from quasars are to be from small volumes in the neighbourhood of large masses. Thermonuclear reactions cannot do, but energy release by gravitational means is a possibility.

The most promising physical model involves gravitational energy release by the accretion of matter onto some massive object-usually a black hole (Rees 1984). The matter is assumed to come from gas and stars orbiting the black hole and may form an "accretion disk" (Begelman 1985) around it while being torn apart by strong gravitational fields near the center. The conversion of gravitational energy of gas accreted by this black hole into radiation may be observed at least as the rest mass equivalent of the infalling material (Perry 1985). In principle accretion by a black hole of mass M and Schwarzchild radius R_s[6] may release an energy of GMm/R_s per unit of accreted mass m. Using $R_s = 2GM/c^2$, we see that the kinetic energy gained

[5] $1L_\odot$ =one solar luminosity ($\sim 4 \times 10^{26}$W) and $1M_\odot$ =one solar mass ($\sim 2 \times 10^{30}$kg).
[6] The radius at which the escape velocity from M reaches the speed of light.

by the mass m falling from a large distance towards the black hole approaches the limit $0.5mc^2$, this may be transformed into radiation by various thermal or non-thermal processes induced by the high velocity infalling gas. Thus assuming hypothetically a complete conversion of kinetic to radiative energy, a mass m can yield as much as 50% of its total rest mass energy just by falling. Luminosity studies predict that black holes or compact objects of mass 10^7-$10^9 M_\odot$ may be present in quasars. Calculations by Gunn (1979) have shown assuming a 10% efficiency for the fueling process, an infall rate of about $1.5M_\odot$ per year is required to fuel the accretion disk in a typical quasar.

Evidence for black holes in quasars is indirect. Although not very compelling, the black hole hypothesis is the most favoured of all models. Strong evidence is provided by the existence of relativstic jets in about 0.1% of known quasars (Cohen et al.1983). These appear to be directed and collimated winds of plasma and magnetic fields (Owen 1985) and are most often seen via their continuum radio emission, they are believed to extend for about 10-100Mpc[7] from the central source (see figure 3). While the origin of such jets is unknown, their presence is evidence for some type of explosive emission which is directed out some "funnel" in the thick accretion disk (figure 5). The presence of broad emission lines in many quasar spectra indicate that large turbulent velocities exist, suggesting the existence of a deep gravitational well-possibly a black hole.

Another alternative model involves the use of multiple supernova explosions. The energy released in a typical supernova explosion is $\sim 10^{45}$J and and hence to produce $\sim 10^{40}$W of power requires about one supernova per day (10^5s). Since the average lifetime of a star is $\sim 10^6$years before it explodes, this model requires that the stars be born at a rate of about 1 per day. Thus this model presents a difficulty because such a rate is needed to be sustained over the lifetime of the galaxy which is highly unlikely. This model is often referred to as the Terlevich model (Terlevich & Melnick 1985) or sometimes the "Starburst model", which is more often applied to an event whereby an intense burst of star formation is occuring at a rapid rate (Weedman 1986). Any dust associated with the star forming region will be heated by strong stellar radiation which re-radiates a strong infrared continuum. Many AGN and possibly quasars detected as "strong" infrared emitters are

[7]Mpc⇒one megaparsec where 1 parsec≈ 3.26 light years.

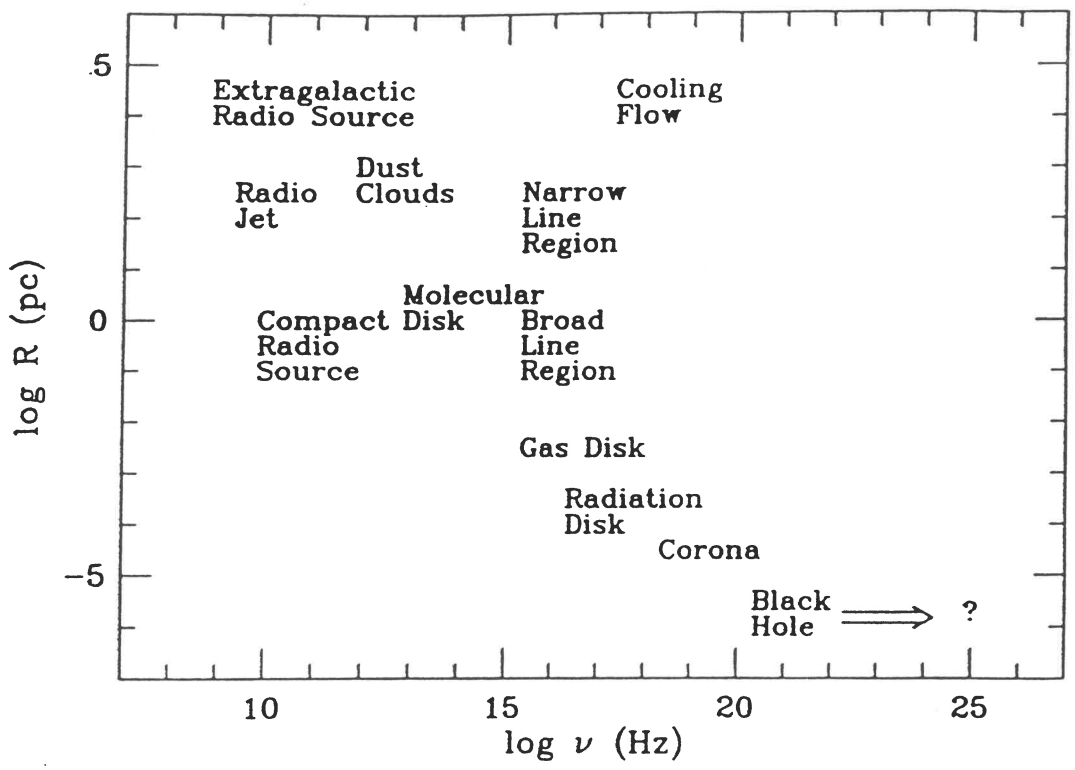

Figure 2: Model showing active components in AGN with the general inverse relationship between energy and scale, note that such a scheme is in close agreement with observations from $10^2 pc$ outwards (R.Blandford *AGN* 1990).

believed to be powered by some starburst process.

The evidence of an observed quasar continuum and emission lines has been well understood as emission from a central accretion disk, reprocessed by a more or less continuous warped disk of material extending for a few parsecs to the outskirts of any existing host galaxy (Sanders et al.1989) (see figure 5). From this interpretation it has been useful to model the activity from quasars and other AGN in terms of discrete well defined zones from which higher energy radiation can be seen to emerge from smaller scales (Blandford 1990). This is illustrated in figure 2, the sequence shows in particular two regions that are believed to give rise to the different extents of line broadening observed in the optical (Wills et al.1985) (see figure 4). These are referred to as the"narrow line regions" (NLR) and "broad line regions" (BLR). Line broadening may be the result of radiation passing through these regions each composed of gas clouds differing in density and velocity. The broad line components in a spectrum being due to emission from 1pc scales-a region of higher electron density closer to the central ionising source than that from which the narrow emission lines are believed to be emitted-less dense regions on 10^2pc scales. These emitting regions hide the central ionising continuum making its study difficult. Their location is determined from the

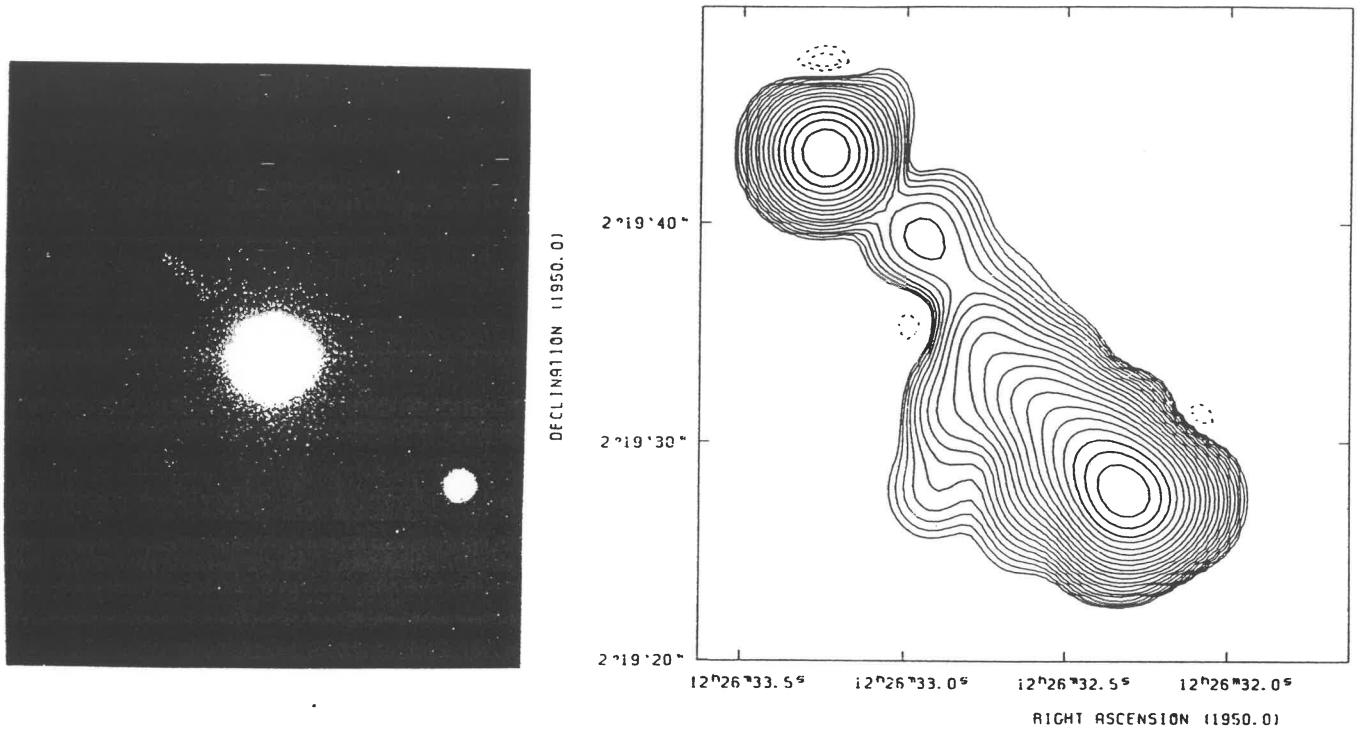

Figure 3: The quasar 3C 273, having redshift of $z = 0.158$, first identified optically by Harzard et al. in 1963. Note the faint jet which extends for about 1 Mpc from the source. On the right is a high resolution radio map at 151 MHz showing a blob of material moving away from the nucleus, the contours represent lines of equal radio flux increasing towards the centre (R.Davis 1985 Jodrell Bank. *IAU Symp.No.119 p.212).*

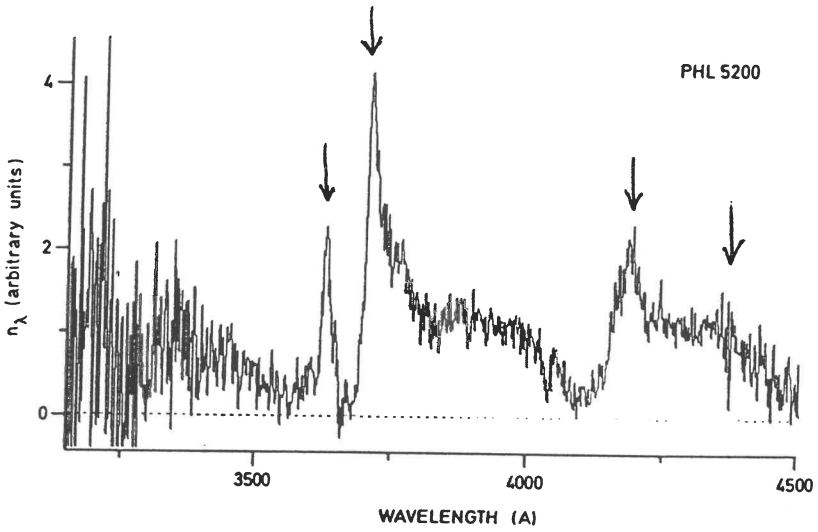

Figure 4: Spectrum of the quasar PHL 5200 at $z = 1.98$ (identified by Lynds,1967) showing broad absorption bands, these bands extend from $z \approx 1.86$ upto 1.98 indicating that the absorption systems are located close to the quasar, along our line of site. The peaks at 3600Å, 3720Å, 4150Åand 4620Åare identified as corresponding to Lyα(1216Å), N(1240Å), Si(IV)(1343Å) and C(IV)(1548Å) emissions respectively in the rest frame of the quasar. Quasars known to posess such Broad Absorption Line Systems are commonly referred to as "BALS". (A.Boksenberg, *IAU symp.No.74, 1977 p.197).*

different periodic variabilities observed in the emission lines (Perry 1985). On the smallest scale (μpc), the existence of a supermassive blackhole accreting matter at extreme relativistic velocities may give rise to large magnetic fields required for the intense synchrotron emission of UV-radiation, X-rays and γ-rays. The anisotropic obscuration by a dusty torus extending to ~ 1 Mpc may account for any beaming of this primary continuum radiation.

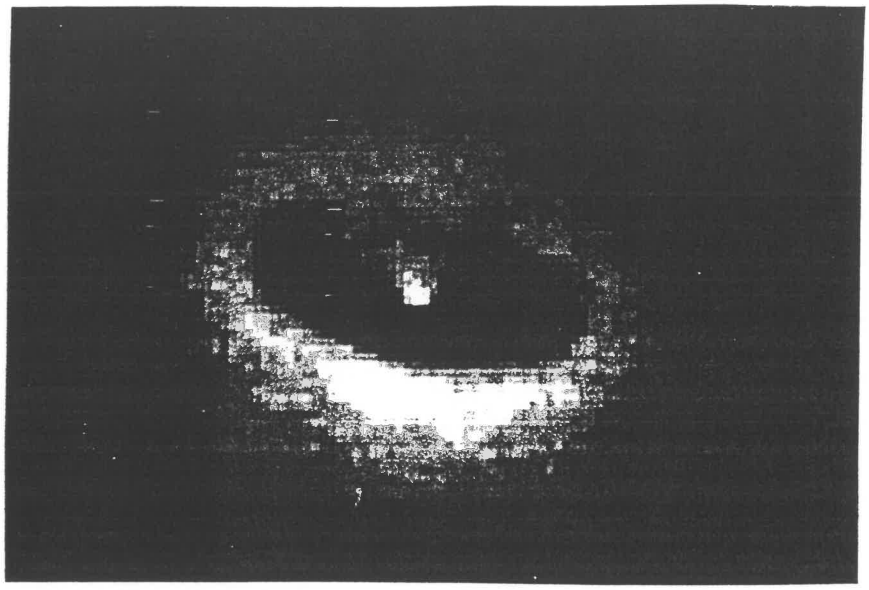

Figure 5: NASA Hubble Space Telescope image of NGC 4261 in the Virgo Cluster located 65 million light years away shows evidence for a disk of cold gas and dust fueling a suspected black hole. The diameter of the disk is estimated to be of the order 100kpc. Image taken at visible wavelengths, Nov.19 1992.

1.4 Quasars and Cosmology.

The ability to observe quasars at a large range of redshifts provides a useful tool to trace the evolution of the universe-in particular the evolution of galaxies. The fact that light speed is "finite" enables us to relate any observed object with the past, in particular the evolution of the properties of objects in cosmic time can be related to an observed variation of the same properties with distance from us. An importance of discovering high redshift quasars is that under cosmological interpretations, redshifts of $z > 4$ will represent a "look-back" time of more than 75% of the age of the universe (10-25 billion years from present day cosmological models). They provide a direct glimpse of the universe as it existed such times ago provided that their redshifts be interpreted as cosmological-as a minority of astronomers have questioned (Burbidge et al.1990). The true z-distribution of quasars needs to be determined before we can study the evolution of some observable property. This has been a difficult task because ever since their discovery, it has appeared from number counts that the space density of quasars versus z

has an apparent peak between $z = 2$ and $z = 3$ and gradually decreases from thereon as shown in figure 6. Schmidt (1989) proposed that the fact of such a quasar population change with redshift may be explained as corresponding to an epoch when most bright galaxies were formed. Or it may be that as the universe expanded to its current stage, the overwhelming majority of quasars became so far away that there may have not been enough time for their light to reach us, they may "burn" themselves out before it does. There is a belief that all galaxies may have gone through a phase in which their nuclei were active, evidence is provided by the observation of very low-level quasar-like activity in the nuclei of many spiral galaxies (Fillippenko et al.1985).

The method by which we can study the space density and evolution of quasars is by use of their "luminosity function". This quantity describes the number of quasars per unit volume as a function of their luminosity. Since observations are always limited to some magnitude, there will always remain the possibility that objects exist which are fainter than our ability to see . Because of this limitation, the luminosity function is applied to a restricted class of objects all of which are brighter than a given cutoff luminosity or absolute magnitude. The basic idea in calculating the luminosity function for a flux limited sample of quasars, involves listing the total number of quasars detected brighter than some absolute magnitude M (which is found from apparent magnitude and distance) within some redshift interval Δz. The volume of the shell containing the quasars (assuming the survey covers all 4π steradians) can be found from $V = \frac{4}{3}\pi d^3$, where d follows from Hubble's law (see section 1.1). Note that here I am assuming an ideal "flat" geometry, though certain corrections will have to be made when dealing with large redshifts due to an expanding universe, these will not be discussed. Repeating this process for different limiting magnitudes leads us to the luminosity function denoted by $\Phi(M)$ which is often represented as a curve as in figure 6. $\Phi(M)$ generally has the units "number Mpc^{-3} brighter than M".

The use of the luminosity function is facilitated by studying its "evolution", this is often done by examining the behaviour of the curve $\Phi(M)$ at different redshift intervals or in other words its "evolution"as shown in figure 6. The curve $\Phi(M)$ can evolve by two means-either by "luminosity evolution", "density evolution" or both. The former case is observed as a horizontal shift in $\Phi(M)$ from a higher redshift (earlier epoch) to some lower redshift (later epoch). Similarly a "pure" density evolution can be seen as a vertical shift between any two epochs. Thus the case in figure 6 suggests

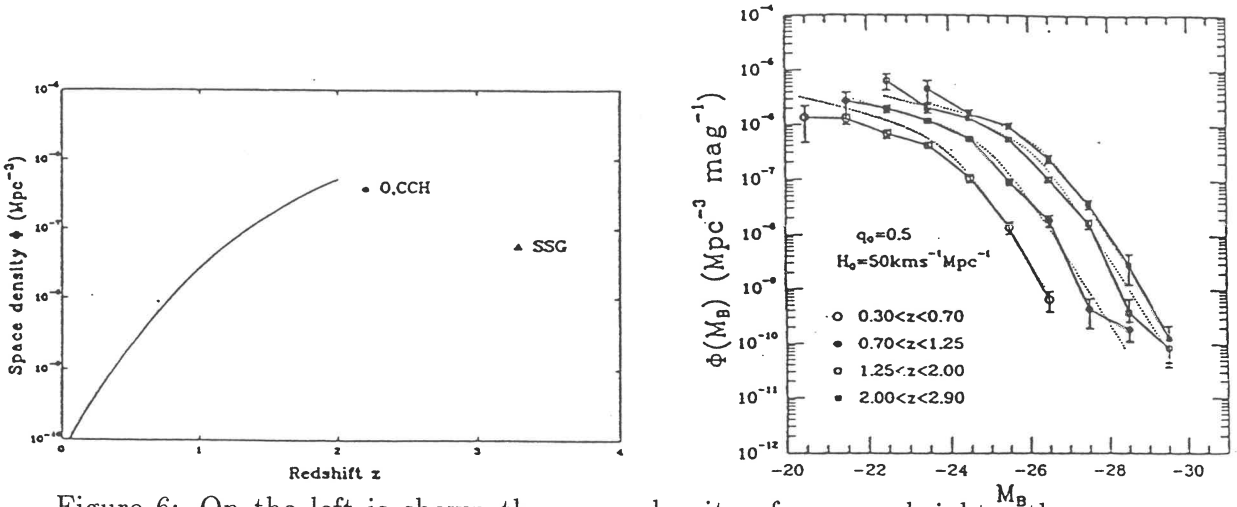

Figure 6: On the left is shown the space density of quasars brighter than absolute magnitude M=-25.9, the curve, circle and triangle represent data from different surveys (Warren & Hewitt 1990). On the right are the quasar luminosity functions for $z < 3$ (Boyle et al.1988).

that there is a slight domination in luminosity evolution-implying that the chance of finding a highly luminous quasar increases with z. It can be seen that the curve corresponding to $2 < z < 2.9$ appears to show a decline in the space density towards lower luminosities ($M > -26$), Boyle (1992) has interpreted this as a flaw in the optical survey used to construct this luminosity function-i.e. it appears to be more incomplete towards fainter magnitudes. Such incompleteness makes it uncertain as to whether quasar evolution should be modeled according to a population evolution or an evolution in the sources themselves-i.e luminosity or it may be a combination of both. A correct solution cannot be confidently found until a substantial amount of high redshift data becomes available and this may be some time yet.

1.5 Optically obscured quasars-Dust ?

The high radio positional accuracy that can be obtained for radio quasars (up to 1" in both RA. & DEC.) has helped to identify them and the associated optical image always seems to coincide with the radio position. A careful comparison with optical images and spectra of the detected radio sources is necessary for quasar identification. Though there have existed a significant number of objects identified initially as flat spectrum radio sources (Condon et al.1977) that remained optically unidentified, such sources were listed as empty fields to a limiting magnitude of 20. Some years ago, several of these objects were later identified at infrared wavelenths (Rieke et al,1979), this

prompted a study of the spectra of such objects to determine whether they were exceedingly "reddenned" thereby explaining why they may have been missed in the optical. Comparison of these sources with previously optically identified ones from the Palomar Sky Survey (1965) showed that they were in fact exceedingly red in color. Observations by Rieke et al. have also shown that samples of quasars found by optical means (not sufficiently dimmed) are biased against sources that are bright in the infrared, even if identifications are made without regard to color. The infrared emitters appeared to be quite distinct with regards to their spectra, they appeared to have very steeply falling spectra within the infrared region ($\alpha \sim 3$)-very different from the IR slopes of optically detected quasars which were characterised with spectral indices of $\alpha \sim 1$. It was believed that more advanced infrared techniques were needed in order to remove this bias. In this project, an alternative explanation will be investigated-it may be that these empty fields are those objects that are greatly obscured by dust. They may also be at very large redshifts.

Quasars are typically about 100 times as bright at optical wavelengths as galaxies and there is no reason in principle why these highly luminous objects cannot be detected out to redshifts $z > 5$ (provided they exist) thereby enabling us to study the evolution of systems over more than 90% of the time since the big bang. The lack of success in finding these high redshift quasars in particular beyond $z > 3$ led Ostriker & Heisler (1984) to investigate whether the possibility that obscuration by dust either in intervening galaxies or intrinsic to the quasar can be responsible for such a decline in observed numbers. Their models are based on using hypothesised "dusty galaxies" along the line of sight to a quasar. They conclude that dust may be an important mechanism for producing the observed behaviour in the luminosity function at high redshift and that the true space density may not decline until much higher redshifts. The empty fields (The compact "flat spectrum" radio sources) may represent a major proportion of these "missing" high redshift quasars. Having no optical counterpart, their redshifts cannot be determined, but their presence may provide the necessary tool to study the effects of dust. Imaging them in the infrared will provide the best test, in particular if they show steep optical-IR spectra then they are believed to characterise a heavily obscured sample of objects-possibly quasars. These methods will be used to identify our selected empty fields.

1.6 This Project.

In this project candidates for observation in the infrared will be selected from empty fields in the Parkes 2.7 GHz radio survey (Bolton et al.1979), all of which will be of the flat spectrum type (ie with $0 < \alpha < 0.5$ in the radio). As discussed earlier, observations have shown that most of the flat radio spectrum sources turn out to be quasars-compact radio emitters. This is the reason for basing our observations on "flat" spectrum radio sources, as there is a higher probability that our identified sources will be quasars.

A sample compiled by A.Savage (1990) contains radio sources from the Parkes catalog classified as empty fields beyond the 23^{rd} apparent magnitude limit. Previous observations of empty fields in the IR have been succesfully carried out from radio surveys limited to optical magnitudes of 20 (namely to the limit of the Palomar optical survey by Rieke et al.1979). Thus empty fields in the Parkes catalog are likely to provide stronger evidence for the possibility of obscuration by dust if an IR detection is made due to the fainter limiting magnitude to which optical identifications have been made.

The following method of study will be undertaken :

I will test the hypothesis that the spectra of many quasars are affected by dust, either in intervening mass concentrations, or within the central parts of the quasar. This may be observed as an affect on the slope of the observed continuum radiation.

Predictions :

As we know, the radio emission from quasars is unaffected by dust[8] Thus a sample of quasars selected by their radio emission should be unbiased with respect to absorption by dust, providing a precise measure of the effects of dust. It is predicted that radio quasars previously catalogued as empty fields, may be precisely those quasars effected by dust. Hence, such quasars have a higher than usual probability of being gravitationally lensed (see section

[8]The opacity of a material can be approximated as $\tau \propto \frac{1}{\lambda}$ (optical depth), dust is more "opaque" to higher frequency radiation and is extinguished the most.

2.1), since their radiation must traverse regions of high mass density. Such quasars may be also be at a very high redshift.

Thus the prediction is that many of the empty fields are either high redshift quasars, or those quasars effected by dust. Hence they will be consistent with the predictions of the unified models discussed above.

Observational :

Flat spectrum radio sources will be imaged in the IR, to see if they are IR bright. If they are, spectra will be taken to see if an identification can be made. Images at different IR bands will also be made of all unidentified sources to see if they can be identified at any specific IR wavelength.

Theoretical :

The composite spectra of Francis (1991) and McDowell (1993)(personal communication) will be used. The Francis composite in particular is an average spectrum constructed from the spectra of 718 quasars taken from the LBQS catalog (Large bright QSO survey). It contains most of the properties expected in a quasar spectrum. This composite spectrum will be used to predict infrared colour-band magnitudes of quasars with changing redshift. The results will then be compared with the data from observations of sources in the Parkes sample at the AAT (Anglo Australian Observatory).

2 Motivation

In this section I will highlight the major purposes and implications for undertaking a study of optically obscured quasars (or optical "empty fields") and why it may be interesting to look for the effects of dust and/or other intervening matter on the quasar spectrum. The important question to consider is: Why do there exist radio sources which have missed detection in the optical? Our hypothesis is that such sources may represent a heavily obscured sample and as such they are predicted to be excessively redenned in optical-infrared color.

2.1 Quasars as probes of the intervening medium.

Once it is established that quasars are at "Cosmological" distances, it has been possible to use them as probes of the intervening medium: either absorption by gas and dust along the line of sight and gravitational lensing by compact or massive bodies. Quasars allow us to probe 80 or 90% of cosmic history - a period spanning the later stages of galaxy formation (Rees 1985). The importance in explaining the existence of heavily obscured sources may aid us in understanding the nature and origin of this intervening medium.

Absorption lines: intervening gas clouds

The utility of the quasars in providing a backlighting source to probe the intervening medium may yield information on the redshift distribution and densities of gas clouds, believed to be composed mostly of neutral hydrogen. Such a medium may absorb and/or reradiate high energy photons emitted by the quasar so that high resolution quasar spectra may reveal features relating to these processes. If intervening gas clouds of hydrogen fill the universe, then there is no way to see them other than with absorption lines in quasar spectra. The existence of narrow absorption lines from neutral hydrogen known as the Lyman-α "forest" lines, have provided a useful tool to set upper limits on the hydrogen gas content of intervening clouds (Fall & Pei 1989). These lines extend from the redshifted Ly-α emission line: $(1+z)1216$Åblueward towards the atmospheric cutoff at 3100Å. This indicates that such clouds are distributed at a large range of redshifts (see figure 7).

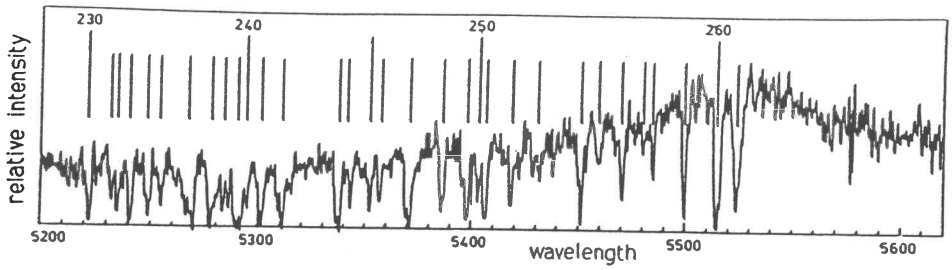

Figure 7: The spectrum of the quasar 1442+101. The Ly-α emission line is at 5523Å. All of the 261 absorption lines blueward of the Ly-α emission line are actually Ly-α absorption lines at smaller redshifts, produced from intergalactic clouds along the line of sight to the QSO (Peterson 1985).

It is questionable whether the empty fields represent those quasars heavily obscured by large amounts of neutral hydrogen either in dense, isolated (possibly primordial) clouds or in the disks of unobserved intervening galaxies (Fall & Pei 1989). This may explain the existence of an absorption trough from the UV throughout the optical region of the spectrum, thereby reducing the optical flux considerably. The presence of dust associated with the Ly-α absorption systems may also contribute to the obscuration. Both scattering and absorption will then contribute to the extinction, the effects from the dust may be observed as a "redenning" of the background quasars. Knowledge on the distribution and nature of intervening gas clouds may aid us in understanding how such clouds become confined and how they may relate to galaxy formation.

Gravitational lensing by galaxies and "Dark matter"

There are several known cases of quasars whose light has been deflected by intervening masses such that observers will see multiple images of a given quasar (see figure 8). Gravitational lensing is often demonstrated by finding a pair of quasars, each of which has the same redshift, but which are separated in the sky by about 2 arcsec. If the spectra are identical then the images correspond to a single quasar being lensed by some forground object. Such lensing by mass concentrations in galaxies, halos and clusters offers an important probe of the intervening medium including the possible amount of "dark" matter which cannot be detected optically but only by its gravitational effects.

In the few quasar lenses observed, a galaxy and/or galaxy cluster has often been seen that provides the necessary mass to explain gravitational lensing (Young et al. 1980). If quasars are optically obscured (and reddened) due to their light passing through galactic disks or regions of high mass density,

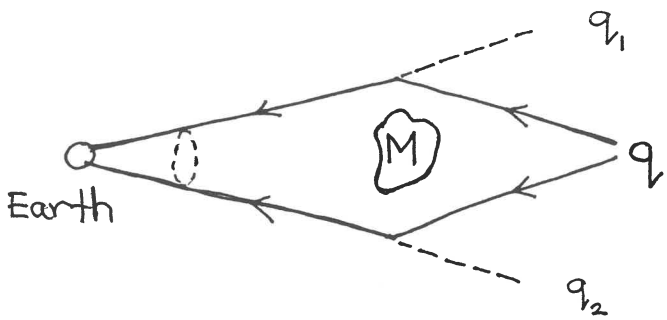

Figure 8: The geometry of a simple gravitational lens with the lensing object of mass M and source (quasar) q.

then there is a significant chance that such quasars will also be simultaneously lensed. Any empty fields being associated with lenses in the radio is a strong indication that they are actually quasars being observed through galactic disks.

There has been one gravitational lens candidate discovered as a strong radio source (MG0414+0535), (Hewitt et al. 1993), which shows its three radio components to be exceedingly red in color. Each component dislays an optical-IR spectral index of $\alpha \sim 9$. It is believed that significant extinction by dust may simultaneously explain the unusually red color and possible absence of optical flux from the lensing object (or objects) responsible for the lensing.

2.2 Unified Models.

One of the goals in classifying all types of active galaxies today is to describe the different forms of activity observed in terms of a single common type of object which is simply observed from different perspectives. The different types of AGN being defined according to the geometrical orientation of this single object, such as the angle to our line of sight of any jet or obscuring dusty torus (Antonucci 1993). The apparently different forms of AGN may also represent different evolutionary stages of the same object, for example, quasars may evolve into seyfert galaxies and so on. These ideas are commonly referred to as "unified models".

The implications for the unified models of quasars is that they may also be related to other AGN through evolution and/or geometry. Though heavily obscured sources may be difficult to account for if their obscuration is due to intervening matter along the line of sight, while intrinsic obscuration may be explained in terms of thick dusty tori. A knowledge of the effects of intervening matter in obscuring distant sources may shed light on the relation

of quasars to nearby AGN. Such extrinsic effects may be incorporated into AGN classification to further establish the unified schemes.

2.3 The "True" intrinsic continuum.

A major problem of present day quasar research concerns the form of the primary emission of the continuum radiation. How much of this primary continuum we can see or expect to see depends on the effects from any intervening matter on this continuum. The presence of dust in or around quasars may have several consequeces. Reddening by dust would alter the intrinsic emission line intensities and hence change the continuum shape. If most of the dust is present within emission line regions, or between the source of ionising radiation and any emission line region, it would modify the expected strengths and profiles of emission lines expected in quasar spectra (McKee 1974).

The nature of the intrinsic quasar continuum may be deduced from observed continua, provided both extrinsic and intrinsic effects from dust and other matter is known. A study of excessively reddened sources where obscuration due to dust is most likely, may aid in determining how such "interfering" effects prevent us from modelling the quasar emitting regions with certainty.

2.4 Redshift cutoffs and evolution.

A consequence of obscuration by intervening matter is that it may seriously bias the observed counts of optically selected quasars at high redshifts (Ostriker & Heisler 1984). The obscuration, if severe, could also distort our picture of quasar evolution. Sufficient detection of enough dust to obscure cosmologically distant is required to explain the observed fall off in quasar numbers found per unit redshift interval beyond a redshift of $z \approx 2.2$ as previously discussed.

It is important to establish the true z-distribution of quasars since the study of their basic evolutionary properties requires the use of complete samples covering the largest possible redshift and magnitude ranges. So far, optical surveys have appeared to be incomplete in establishing the quasar

luminosity function and its evolution for $z > 3$. It is likely that redshift estmates for a significant number optically faint radio sources (Dunlop et al. 1989) may provide evidence for a higher z-cutoff and hence enable a detailed study of the luminosity function at high redshifts.

The highest known redshift has grown rather slowly as a function of the total number of quasars discovered, leading to conjectures that perhaps there does exist a real cutoff before which the quasar birthrate was small. i.e. the fact almost none are observed with $z > 4$ may imply that very few existed then, with the majority being born at much later epochs.

Heavily obscured samples need to be examined more closely if we are to determine the true epoch of quasar development.

3 Previous Work

3.1 IR continua, Dust and Intrinsic obscuration.

About a third of the total luminosity of a quasar or Seyfert galaxy is emitted in the range $1 - 100\mu m$ (near-far infrared) (Sanders et al. 1989). The emission mechanism is not as yet established, an attractive possibility is thermal reprocessing of the optical to far UV from the primary continuum source by nearby dust, as originally proposed for some Seyferts by Rees et al. (1969).

Some indirect evidence supporting such a hypothesis include a spectral turnover usually within $\lambda < 3\mu m$ (see figure 1) (Neugebauer et al. 1979; McAlary & Rieke 1988) and also at $\lambda > 100\mu m$ (Barvainis 1987). The sharp cutoff for $\lambda < 3\mu m$ (at about $1\mu m$ or $10^{14.5}$Hz in fig. 1) is believed to be a result of a constant sublimation temperature at which dust grains can still survive (~1500-2000K) (Malkan 1989). The turnover at $\lambda > 100\mu m$ is made to correspond to lower grain temperatures (~30K). Thus the long and short wavelength bands of the IR quasar spectrum has generally been explained by dust models according to the maximum and minimum temperatures that grains can attain. There is a lack of flux variability and polarisation throughout the IR (Edelson & Malkan 1987) as compared with the emission at $\lambda < 1\mu m$. The existence of steep infrared spectra (with $\alpha > 3$) is the best indication for a "reddened" continuum (Rieke et al. 1982). Some excessively reddened sources have also revealed themselves via silicate spectral features (Cutri et al. 1984). These observations provide strong evidence that dust be associated with quasars.

Calculations have shown that the IR continuum can be fitted with a dust model in which the dust is in a warped accretion disk (Malkan 1989) and contributes a thermal continuum. Such optically thick disks will make it almost inevitable that some reprocessing of the nuclear UV-optical continuum by dust must occur. The absence of optical flux is very easily accounted for if such a dust distribution is axisymmetric (i.e. as in a disk or torus) (Barvainis 1992). If the quasar nucleus is visible at all, it will be largely unreddened. If on the other hand our line of sight to the nucleus passes through an obscuring torus, the object may not be identified as an "optically luminous" quasar but

as an empty field, detectable only by the presence of radio and/or IR emission (Rieke et al. 1979).

3.2 The Obscuration Hypothesis.

The possibility that dust can be used to explain the majority of IR emission from quasars, has lead researchers to investigate whether extinction by "large" amounts of dust in intervening galaxies (or within the quasar) can account for the decrease in observed counts of optically selected quasars at high redshift (Fall & Pei 1989; Ostriker & Heisler 1984; Heisler & Ostriker 1988).

Wolfe et al. (1986) have observed that in some high redshift quasars, Lyman-α absorption lines (see figure 7) are broadened by radiation being damped by dust. These lines are believed to be the signatures of the disks of spiral galaxies at an early stage of evolution (Fall & Pei 1989), since they have also been seen to be associated with heavy element absorption lines (Peterson 1985). The presence of heavy elements in Lyman-α clouds implies that they have been enriched by stellar material and hence make their presence in intervening galaxies. The "damped" Lyman-α systems are primary candidates responsible for most of the obscuration of distant quasars. It is estimated that the total mass of neutral hydrogen in such systems is comparable with that in all forms of luminous matter observed today (Fall & Pei 1992).

Fall & Pei (1989) have compared the spectroscopic properties of quasars with redshifts $2.75 \leq z < 3.4$ with and without damped Lyman-α systems present in their spectra. Using galactic extinction curves from the Milky Way, Small and Large Magellanic clouds to represent the properties of the dust, they find the following upper limits for the dust to gas ratio in such systems: 0.20 ± 0.07 (MW-curve), 0.06 ± 0.02 (LMC-curve) and 0.04 ± 0.01 (SMC-curve). Fall & Pei (1989) interpret these values as "typical" dust to gas ratios in the damped Lyman-α systems. Using these values they find that the mean optical depth due to dust in these systems along random lines of sight to quasars at high redshift cannot account for the observed behaviour of the high z quasar luminosity function. The analysis of Fall & Pei (1989) was based on the use of upper limits on the observed reddening in quasars with damped Lyman-α systems only. The possibility of obscuration

by intergalactic dust not associated with Lyman-α systems was ignored. Such dust may represent a major source of uncertainty in their results. The mean optical depth as derived by Fall & Pei is a factor > 2 lower than that adopted by Heisler & Ostriker (1988). Models used by Heisler & Ostriker show that various distributions of dust can in fact lead to severe obscuration of quasars at optical wavelengths.

Using a more sophisticated treatment of extinction due to our lines of sight passing through hypothesised "dusty galaxies", Heisler & Ostriker (1988) use a model in which all the dust is within normal galaxies like our own and another in which it is spread out uniformly through the universe. They predict that if cosmic dust is smoothly distributed, then objects more and more distant are made optically fainter and redder in a systematic way, as observed by Ostriker & Cowie (1981). While they stress that a lumpy dust distribution may not redden distant quasars at all, but actually remove them completely from a sample limited to some optical flux. Although they may still be identified at longer wavelengths such as the infrared.

Heisler & Ostriker (1988) have made a few illustrative simulations of how cosmological dust obscuration might affect optical observations. Their calculations are based on three models: uniform absorption, non-uniform absorption and no dust absorption. The distributions in quasar numbers according to these models are found from calculating the expected luminosity function, with model dependent parameters such as the distribution of absorbers and mean optical depths along lines of sight.

Strong evidence to support the dust model was acheived from predicting quasar number counts in terms of redshift. In particular, the uniform dust model appeared to be the most consistent in reproducing the observed behaviour in quasar number density with redshift (see fig. 9). This model was the best fit to the observations, while the dust-free model predicted more quasars at fainter magnitudes and larger redshifts, overestimating the number density for $z > 0.5$ by almost a factor of two.

Another study undertaken by Heisler & Ostriker which will also be used in the analysis of our observations later on, is whether the proposed dust obscuration by itself, predicts more "color evolution" than is observed. They state that if a significant number of quasars are being removed from a sample by obscuration, then one might expect that the observed ones will be heavily reddened, contrary to observation. Figure 10 shows the mean color $(B - V)$ versus redshift for various dust models. Note larger values of $B - V$ implies

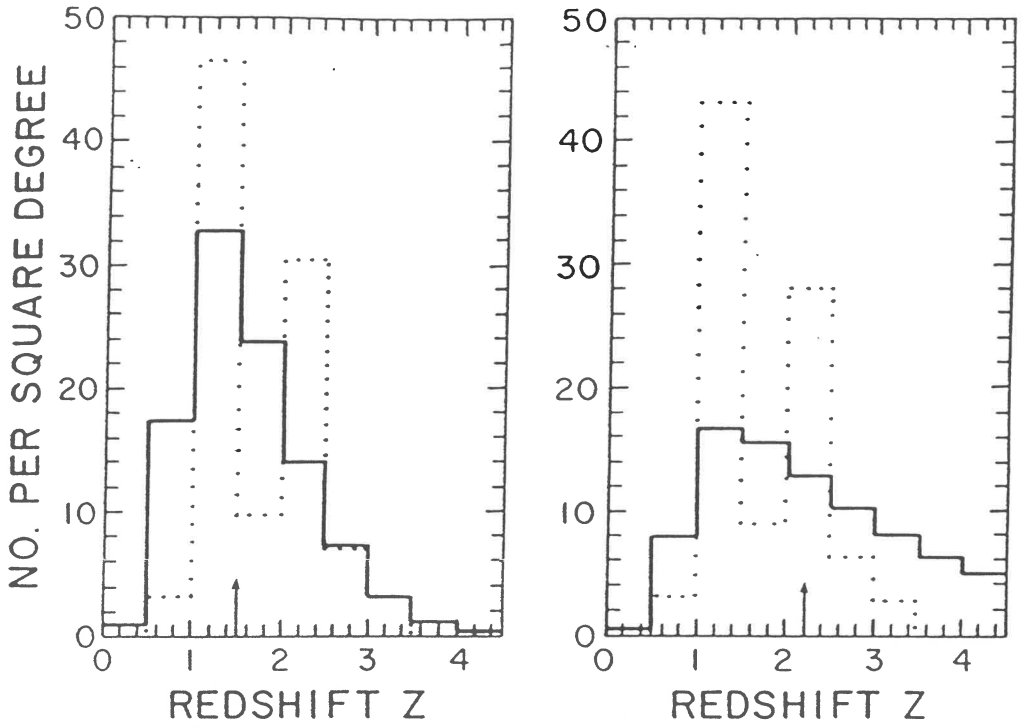

Figure 9: Number of quasars/square degree in the blue magnitude range: $18 \leq B \leq 22$ and Absolute magnitude $M_B \leq -20.4$. Observations from the Koo-Kron survey (1982) is shown in the dotted histogram. Uniform dust model (left) and the dust-free model (right) which predicts too many distant quasars. (Heisler & Ostriker 1988).

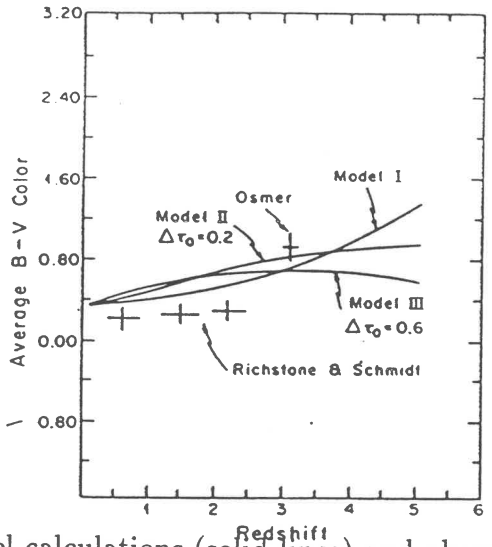

Figure 10: Model calculations (solid lines) and observations by Richstone & Schmidt (1980) and Osmer (1979). Rapid reddening is observed with model (i)-uniformly distributed dust. (Heisler & Ostriker 1984).

a relatively larger optical (V) flux or more reddening. Model (i) (uniform dust) shows as expected an increase of mean color with redshift. Models (ii) and (iii) refer to nonuniform dust models with different adopted comological parameters. Note that these calculations have neglected the "K-correction" (section 4.2)-an effect on the color due to the redshifting of spectral features.

Heisler and Ostriker (1988) conclude that there is considerable evidence in favor of dust obscuration to explain the steep decline in observed quasar numbers at high redshift. They predict that the best test of this obscuration hypothesis will come from a search to find reddened quasars where at present optical-empty field radio sources are detected.

3.3 Detection of Empty Fields.

The fact that spectroscopic identification of most faint flat spectrum radio sources ($\alpha_{radio} < 0.5$) turn out to be quasars, implies that such radio sources which are invisible in the optical, may represent a large majority of quasars. Just how many of these empty fields should be present in radio surveys is an important question to consider.

Surveys have shown that there is a general lack of correlation between radio and optical luminosities (Marshall 1987) and it is not known whether the fraction f of quasars that are radio "loud" ($S_{2.7Hz} > 0.5$Jy[9]) is a constant with redshift. If f decreases with z, then empty fields may not occur as frequently, so that one would expect all radio sources to have optical counterparts unless there is heavy dust obscuration (Ostriker & Heisler 1988). However if f is relatively constant, then high redshift radio quasars will exist and the optically obscured ones could provide a test for dust models. Marshall (1987) has shown that the radio detection rate in an optically selected sample is $\sim 30\%$ for a wide range of optical magnitudes and radshifts up to $z = 3.5$. Such a result is consistent with f being constant and hence we may expect a significant number of empty fields in radio-optical surveys.

The largest number of high redshift quasars detected from a radio sample is from a survey by Savage et al. (1990). The sample was selected from the Parkes radio survey down to a flux limit $S_{2.7Hz} = 0.5$Jy, which covered some 15000 square degrees. Out of a sample of 403 flat spectrum radio sources,

[9]Jansky (Jy)-a measure of radio flux, 1Jy = $10^{-26} W m^{-2} Hz^{-1}$.

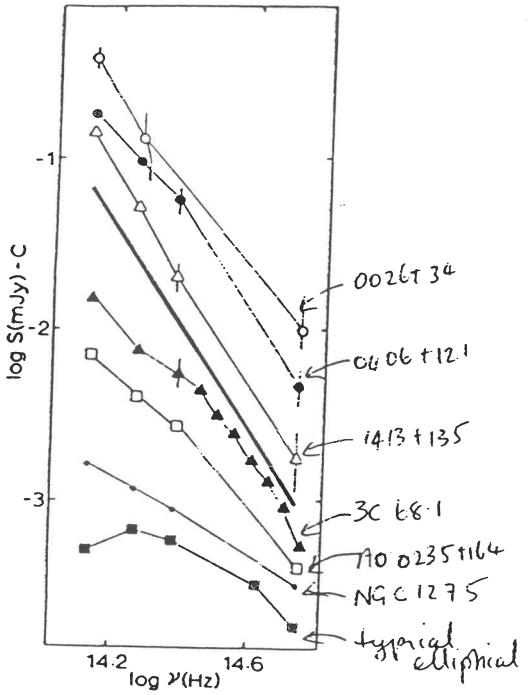

Figure 11: Optical-IR spectra of sources identified by Rieke et al. (1979) and other red extragalactic objects (below the dividing line).

71% were identified with quasars and redshifts have been determined for 85% of these. The other proportion of radio sources have mostly been associated with faint radio galaxies and 51 sources were classified as empty fields, undetectable to a blue magnitude limit of 22.5. Radio sources for infrared imaging in this project were taken from this survey, results are discussed later on.

The work undertaken in this project was initially motivated by observations made by Rieke et al. (1979) having detected six objects in the IR (at $2.2\mu m$) at the positions of flat spectrum radio sources that had missed optical detection to $V = 19.5$. Some of these sources were detected with K-band magnitudes of 15.17 and thus were relatively bright in the IR. They found the remarkable result that the infrared-optical spectra of these sources were described by power laws of index $\alpha \approx 3$. These were much steeper or redder than previously known QSOs as well as other "red" galaxies (see fig. 11). Rieke et al. conclude that these sources missed optical detection because they are exceedingly red in color.

4 Theoretical-Predicting Quasar Colors

In this section I will theoretically predict color indices for a quasar situated at any given redshift. I assume composite or "average" quasar spectra (Francis 1991; McDowell 1993 (personal communication)) and combine them so to obtain a theoretical emitted intrinsic continuum. The necessary corrections to this spectrum are applied to obtain estimates of optical-infrared colors expected to be observed. In general, these colors will be determined as a function of quasar redshift.

4.1 The Francis Composite Spectrum.

In order to adopt an intrinsic quasar continuum (i.e. a $z = 0$ spectrum), it is necessary to use some average continuum shape whose large scale properties are characteristic of all quasars. Such an average must assume that there is some continuity between the spectral properties of quasars of different z and absolute luminosity, so that spectra can be pieced together and a composite formed.

A composite spectrum was derived by Francis et al. (1991) by basically taking quasars at different redshifts and merging the data rebinned to their respective rest frames. Fluxes from all spectra showing common rest wavelength regions were then averaged. This composite (see fig. 12) was built from a large sample of 718 quasars taken from the LBQS catalog (Foltz et al. 1987, 1989; Hewitt et al. 1991). All sources in this catalog were identified with B_J-band magnitudes < 19.

One of the major difficulties in defining the average was that many of the LBQS quasars in the high and low redshift regions showed little or no overlap at all. Each LBQS quasar contained information about a different rest-wavelength region, mainly between quasars of very different luminosity. In order that each component quasar contributed equally to the composite, a normalising method was used in which each spectrum was scaled to some appropriate mean flux before addition. Francis et al. (1991) find that there is significant scatter about the mean variations in the strengths of primary emission lines about the underlying continuum. They also find that such a continuum is "not well represented by a power-law on any but the smallest

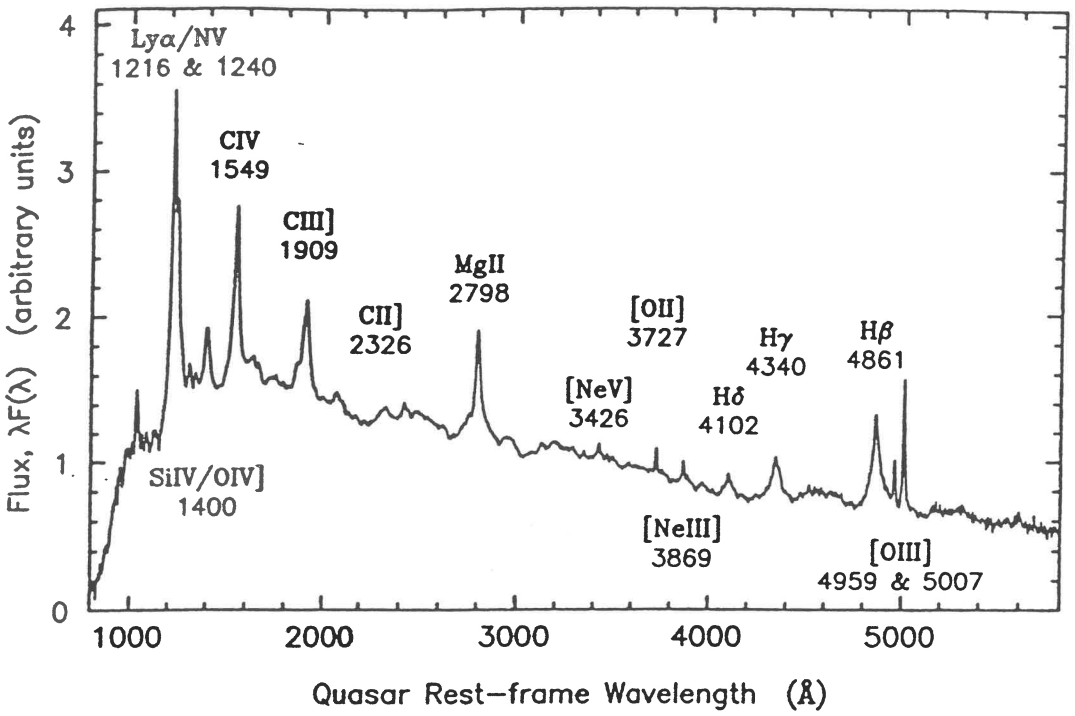

Figure 12: The rest-frame composite of 718 optical quasar spectra showing the strongest emission features. The wavelength range covered by this composite is 800-6000Å. (Francis et al. 1991).

of scales", and on such scales the continuum slopes are found to range from $\alpha = -0.5$ to 1.5, with a common value of α=-0.3.

Such a composite has been used extensively in modelling the emitting regions of quasars as well as establishing new techniques for the selection of quasar candidates at high redshift (Cristiani & Vio 1990). For our purposes, we only require a general intrinsic continuum shape that when redshifted is typical of most quasars observed. Our aim is to determine whether the observed properties of our empty fields actually represent significant deviations from such a composite spectrum, so that the nature of their emission may be attributed to very different mechanisms.

The Francis composite spectrum will be combined with a second composite of longer wavelength coverage when composite quasar colours will be predicted as a function of redshift in the next section. This new composite compiled by J.McDowell (CFA[10])(1993) extends from 0.5 to 286.4μm of which the region from 0.6 to 2.612μm is adjoined to the Francis composite (see fig 17). The purpose of this is to increase the redshift range over which colours are defined (see next section).

[10]Centre for Astrophysics-Harvard

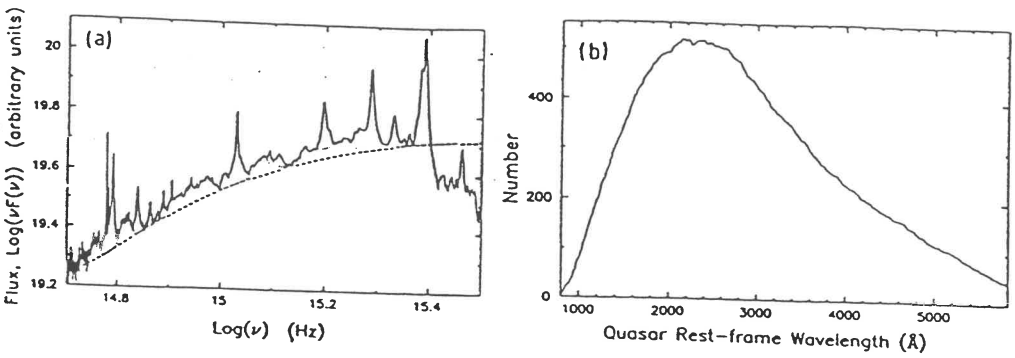

Figure 13: (a) The composite spectrum plotted as $log(\nu F_\nu)$ vs rest frame $log(\nu)$. (b) This shows the number of quasar spectra contributing to the composite as a function of rest-frame wavelength. (Francis et al. 19991).

4.2 Quasar colors as a function of redshift.

Colors are defined via magnitudes which are normally measured through filters that have a bandpass defined by their width in wavelength units. For example the B-magnitude results from the measured flux that enters a filter 1000Åwide and centered about 4400Å. Table 2 lists some standard bandpasses with respective effective central wavelenghths λ_o and bandwidths $\Delta\lambda_o$. The quantities $f_\lambda(0)$ or $f_\nu(0)$ are used when transforming between magnitudes and fluxes. These transformations are made by adopting an arbitrary definition of the magnitude system, which usually sets zero magnitude at all wavelengths to correspond to the flux from the star Vega. The relation that relates magnitudes and fluxes is given by:

$$m_x = 2.5log\left[\frac{f_\lambda(0)}{f_\lambda(m_x)}\right] \tag{4.1}$$

where $f_\lambda(m_x)$ is the flux in $erg\ cm^{-2}s^{-1}\mathring{A}^{-1}$ corresponding to the magnitude m_x in the filter band x.

Note that the bandpasses in table 2 are defined by the availability of detectors sensitive to various spectral regions and on the properties of the filters used. Each bandpass has an associated photometer response function $S(\lambda)$, which usually represents the transmission characteristics of the filter (see figure 14). Atmospheric transmission has also a wavelenghth dependence - most important in the IR where the bandpasses have been defined by re-

Filter Band	λ_o^*	$\Delta\lambda_o$	Absolute Spectral Irradiance for mag = 0.0 $f_\lambda(0)$	$f_\nu(0)$
U	0.365 μm	0.068 μm	4.27×10^{-9} erg cm^{-2}s^{-1}Å^{-1}	1.90×10^{-23} Wm^{-2}Hz^{-1}
B	0.44	0.098	6.61×10^{-9}	$4.27(4.64)+ \times 10^{-23}$
V	0.55	0.089	3.64×10^{-9}	3.67×10^{-23}
R	0.70	0.22	1.74×10^{-9}	2.84×10^{-23}
I	0.90	0.24	8.32×10^{-10}	2.25×10^{-23}
J	1.25	0.3	3.18×10^{-10}	1.65×10^{-23}
H	1.65	0.4	1.18×10^{-10}	1.07×10^{-23}
K	2.2	0.6	4.17×10^{-11}	6.73×10^{-24}
L	3.6	1.2	6.23×10^{-12}	2.69×10^{-24}
M	4.8	0.8	2.07×10^{-12}	1.58×10^{-24}
N	10.2		1.23×10^{-13}	4.26×10^{-25}

* $\lambda_o = \int \lambda S(\lambda) d\lambda \Big/ \int S(\lambda) d\lambda$, where $S(\lambda)$ is the photometer response function.

Table 2: Standard short and long wavelength bandpasses with central effective wavelengths λ_o and bandwidths $\Delta\lambda_o$. Note filter bands from I through to N are defined as IR bandpasses. (Zombeck 1982).

stricted windows where the atmospheric transmission peaks. Figure 14 also includes atmospheric effects.

Color is defined as the magnitude difference in any two bandpasses. In terms of filter properties and measured spectral fluxes, the color index $m_{x_1} - m_{x_2}$ can be formally represented in the following form:

$$m_{x_1} - m_{x_2} = 2.5log\left[\frac{\int_0^\infty S_{x_2}(\lambda)F(\lambda)d\lambda}{\int_0^\infty S_{x_1}(\lambda)F(\lambda)d\lambda}\right] + C \tag{4.2}$$

$F(\lambda)$ represents the overall observed spectral energy distribution and is convolved with the appropriate filter response functions $S_{x_1}(\lambda), S_{x_2}(\lambda)$ corresponding to bandpasses x_1 and x_2 respectively. The limits in the integrals can be replaced by upper and lower wavelength cutoffs defining the bandpasses. C is a normalising constant characteristic of the bandpasses and magnitude system used. From equations 4.1 and 4.2,

$$C = 2.5log\left[\frac{f_{\lambda_1}(0)}{f_{\lambda_2}(0)}\right] \tag{4.3}$$

To predict the typical colors of quasars using the composite spectrum as our intrinsic continuum, it is first necessary to redshift the composite by some arbitrary amount z. From the definition of the redshift parameter z (see section 1.1), we have:

$$\lambda_o = \lambda_e(1+z) \tag{4.4}$$

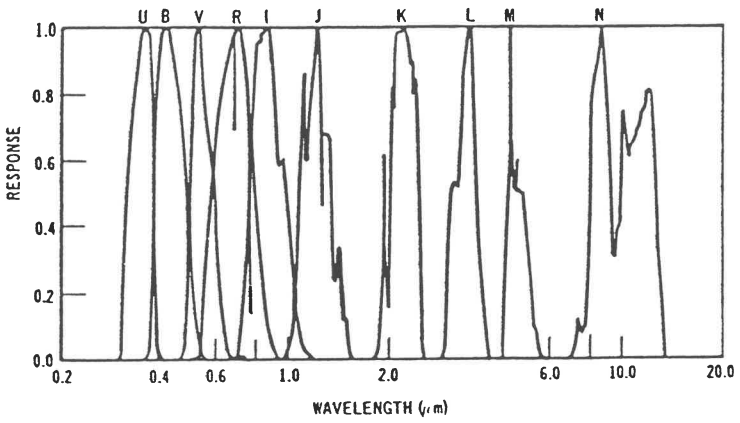

Figure 14: Filter response curves for bandpasses corrected for atmospheric transmission. (Zombeck 1982).

Using this relation, it was possible to transform every wavelength of the composite (λ_e) to an "observable" wavelength $\lambda_o(z)$ for any z. Note that such redshifting not only shifts every spectral feature of the composite by a factor $(1+z)$, but also introduces a "stretching" of the entire spectrum by the same factor. Thus since the composite at $z = 0$ covers a limited wavelength range from 80 to 600nm, it will appear to cover broader wavelength ranges when redshifted by various amounts. (see figure 15).

As a consequence of the gradual redshifting of the composite spectrum, it is evident from figure 15 that the fixed B and R bandpasses admit varying amounts of flux at different redshifts. Thus it is expected that there will be systematic variations in band magnitudes and hence colors due to the shape of the continuum and emission lines in the composite spectrum, which enter the bandpass of different filters according to the redshift. Also, the "stretching" effect associated with the redshift can be represented as an "effective" narrowing of the frequency bandwidth $\Delta\nu_o$ of a certain bandpass. This somewhat reduces the admitted flux that enters a filter band.

A correction will have to be applied that takes into account both these effects as bandpass magnitudes are calculated from the composite as a function of redshift. Both effects are together referred to as the K-correction (Sandage 1975) and is defined as a magnitude correction on a bandpass x as follows:

$$m_x(z) = m_x(z = 0) + K_x \tag{4.5}$$

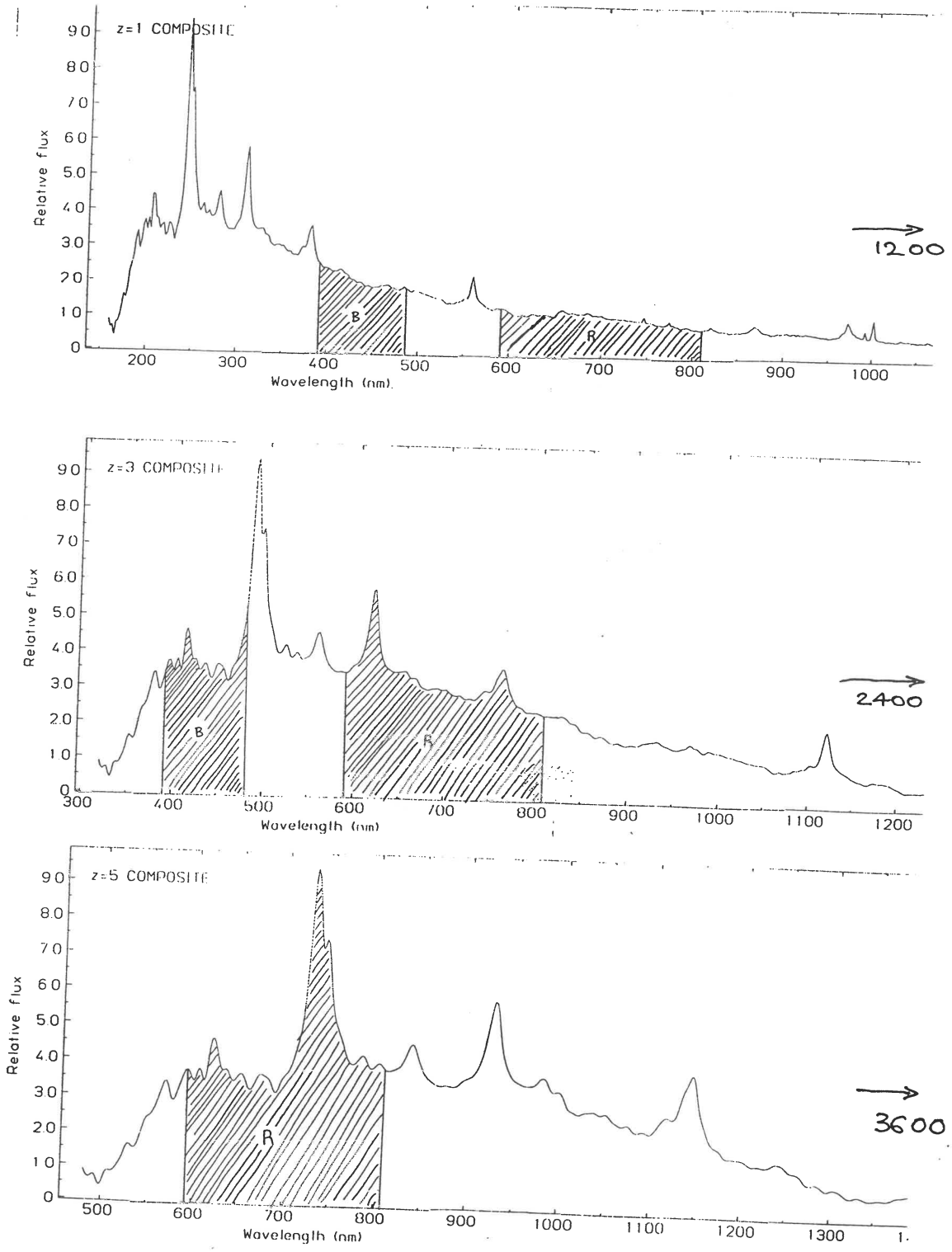

Figure 15: The composite spectrum of figure 12 redshifted by various amounts, showing regions defined by the B and R bandpasses centered on 440nm and 700nm respectively. Also indicated (arrows) are the maximum wavelengths to which the spectra extend.

$m_x(z)$ is referred to as the K-corrected or observed magnitude and $m_x(z=0)$ is the true magnitude due to flux emitted from the same bandpass in the unredshifted spectrum. An expression relating the K-correction to redshift z and integrated fluxes for a particular bandpass x is as given by Cristiani and Vio (1990):

$$K_x = 2.5log(1+z) + 2.5log\left[\frac{\int_0^\infty S_x(\lambda)F(\lambda)d\lambda}{\int_0^\infty S_x(\lambda)F\left(\frac{\lambda}{1+z}\right)d\lambda}\right] \tag{4.6}$$

where the first term represents a bandwidth correction due to a compression of the bandwidth from $d\nu_o$ centered on ν_o to (using $c = \nu\lambda$ and equation 4.4)

$$d\nu_z = \frac{d\nu_o}{1+z} \tag{4.7}$$

for some redshift z. The second term is a correction on the flux that is admitted in the bandpass x, ie due to the fact that radiation received by an observer at a wavelength λ is emitted by the object at $\lambda/1+z$, so that different regions of the spectrum are observed in the measuring bands at diffrent z. $F(\lambda)$ is the observed flux per unit wavelength and $S_x(\lambda)$ the x-filter response function.

Based on equation 4.6, K-corrections have been calculated as a function of redshift for the composite spectrum and results have been plotted in figure 16. Note that these K-corrections are for the specific bandpasses indicated which enter and leave the spectrum as it is redshifted accordingly. Due to the limited wavelength coverage of the composite, a certain waveband will remain under the composite for only a specific redshift range during which then calculations are possible. As shown in figure 16, these redshift ranges for the B, R and K bands are respectively:
$0 \rightarrow 3.5$, $0.6 \rightarrow 5.5$ and $3.3 \rightarrow 21.5$.

It is easy to interpret these plots using equation 4.5. For instance, since most of the flux in the composite spectrum resides in the UV region-ie about the position of the Ly-α emission line (see fig.12), when this region becomes redshifted into any bandpass x, $m_x(z)$ decreases rapidly so that the value K_x drops dramatically becoming negative in some cases. This explains the turnover in the K-corr. vs z plots of figure 16. As for the K-band plot (plot (c)), the Ly-α region can be seen to enter this bandpass at a redshift of $z = 15$!

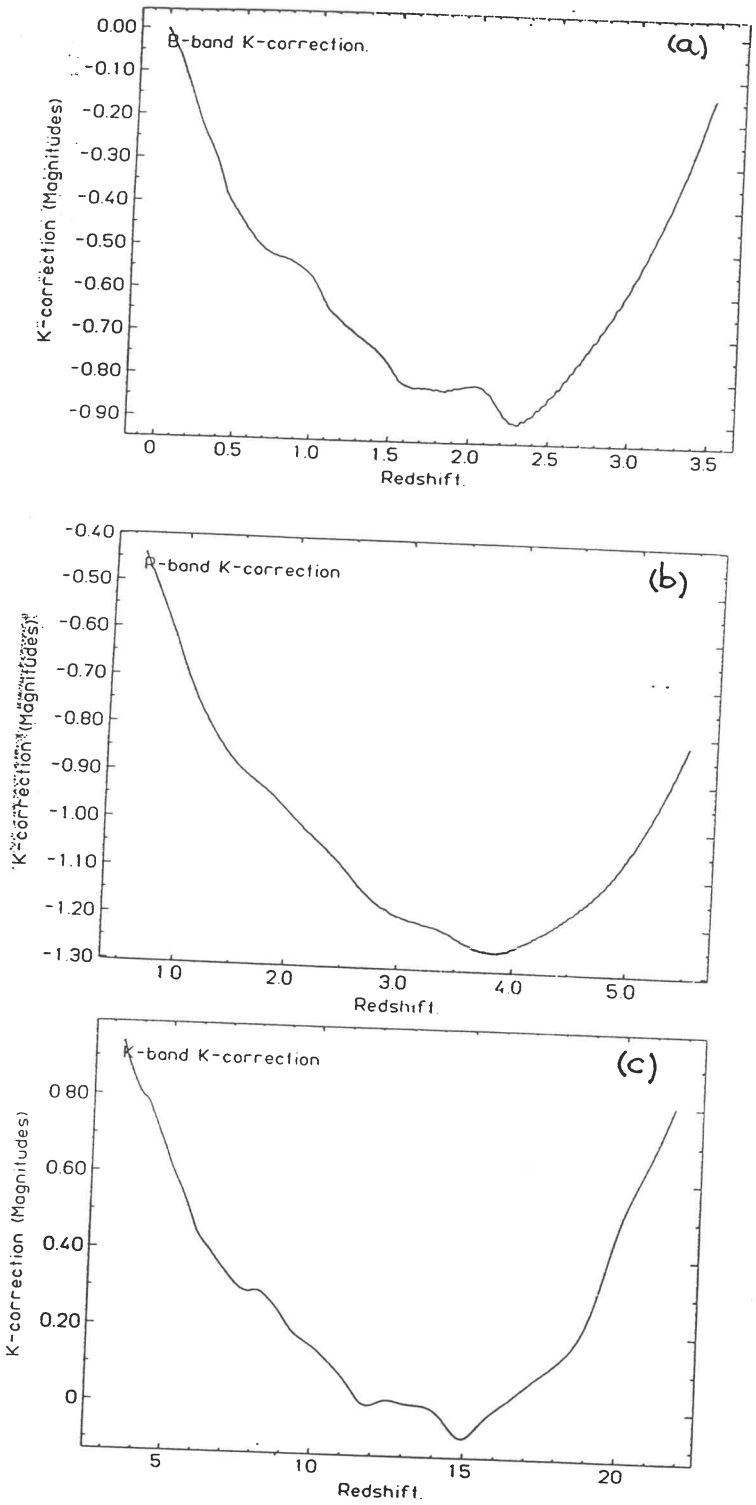

Figure 16: Plots of K-correction vs z for the bandpasses: (a) B, (b) R and (c) K with bandwidths and effective wavelengths as defined in table 2 using the Francis composite spectrum alone (80-600μm). Note the redshifts at which fluxes in each band peak, i.e. minima in the plots.

One further remark on the K-correction is that such a correction is much easier to deal with for non-thermal sources whose continuous spectra are representable by power by laws; that is; intrinsic fluxes can be represented as $f_e(\nu) = C\nu^{-\alpha}$ (C=constant) (see section 1.2). If a source is non-thermal in origin with spectral index α, then from equations 4.4 and 4.7, we have:

$$f_{observed}(\nu) = f_e(\nu)(1+z)^{1-\alpha} \tag{4.8}$$

where $f_e(\nu)$ is the intrinsic flux emitted into a fixed bandpass within which α = constant. If $\alpha = 1$ which is a fairly common value for most non-thermal emitters, then equation 4.8 gives $f_{observed}(\nu) \equiv f_e(\nu)$. Furthermore, equation 4.8 together with 4.6 can be used to determine the spectral index α as a function of redshift for a specific bandpass.

Quasar composite colors as a function of redshift can be directly predicted through the use of the K-correction term of equation 4.6 which incorporates all effects introduced by the redshift. Observable color indices can be written in terms of the K-correction parameter K_x as follows using equation 4.5: For any two bandpasses x_1, x_2 we have

$$m_{x_1}(z) = m_{x_1}(z=0) + K_{x_1}$$

$$m_{x_2}(z) = m_{x_2}(z=0) + K_{x_2}$$

so that

$$m_{x_1}(z) - m_{x_2}(z) = K_{x_1} - K_{x_2} - [m_{x_2}(z=0) - m_{x_1}(z=0)] \tag{4.9}$$

The quantity in square bracketts can be interpreted as an intrinsic color index corresponding to that observed $(m_{x_1}(z) - m_{x_2}(z))$ at any redshift z. This leads us to define the quantity $K_{x_1} - K_{x_2}$ as some "color excess" due to redshifting effects alone. By replacing the terms in equation 4.9 in terms of fluxes through use of equation 4.6, it will directly reduce to equation 4.2.

The purpose of introducing the K-correction is that it will help to visualise the behaviour of quasar colors in terms of redshift. In particular, the color term $K_{x_1} - K_{x_2}$ in equation 4.9 will give a direct indication as to what extent an observed quasar color can be attributed to redshifting effects alone. It is then possible to isolate the effects that may be due to other physical

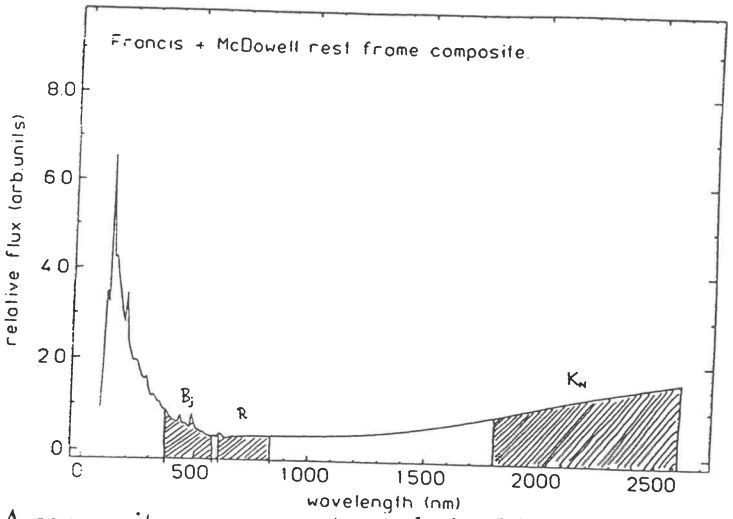

Figure 17: A composite quasar spectrum derived from the composite of Francis et al. (1991) ($0.08\mu m$ to $0.6\mu m$) and the McDowell composite ($0.6\mu m$ to $2.612\mu m$) used for the prediction of quasar colours.

mechanisms-in this case relatively large optical-IR colors will provide strong evidence to support a dust hypothesis.

To predict typical optical-IR colours of quasars as a function of redshift using a composite quasar spectrum, it is necessary that the composite covers an appropriate redshift range so that as it is gradually redshifted, any two magnitude bands that define a certain colour index remain simultaneously within the composite. Redshift ranges defining required colours using the Francis et al. composite alone are not large enough on which to base observational predictions to required redshifts. The $B-K$ color in particular is only defined to within the range $z = 3.3 \rightarrow 3.5$. In order to extend redshift ranges so to make better use of the color vs z plots, I have extended the Francis et al. composite redward past the wavelength 600nm (see figure 12). I have assumed continuity with the composite compiled by McDowell (1993)-(personal communication) which covers a wavelength range from 0.5 to $286.4\mu m$. Joining the Francis composite spectrum at 600nm ($0.6\mu m$) to the first 2 microns of the McDowell composite, our new rest frame composite now covers the wavelength range: 80nm to 2612.89nm (see figure 18). Shown in figure 17 are the bandpasses B_J, R and K_N. The Francis composite has been extended so to include the K_N bandpass, this ensures that our required colours are defined for maximum redshift ranges when they are predicted from the redshifted composite. The new rest frame composite of figure 18 will be used in predicting quasar colours as a function of redshift.

A specific quasar color $m_{x_1}(z) - m_{x_2}(z)$ was determined as a function of redshift as follows: First the redshift range within which the two bandpasses x_1, x_2 are simultaneously present within the composite as it is redshifted is defined so that the relevant calculations can be performed. To further ensure a larger wavelength coverage for a specific color, the standard filter

bandwidths have been reduced by an amount that corresponds to 90% of the flux that enters the standard bandpass. Using tabulated bandwidths from table 3 with equation 4.4, the respective redshift limits defining certain colors were found. Redshift ranges for $B-R$, $R-K$ and $B-K$ colors using our composite are shown in the color vs z plots of figure 18.

Colors are computed by applying equation 4.2 as the composite is redshifted by successive amounts Δz. As noticed from equation 4.2, the redshifted composite flux $F(\lambda)$ is convolved with the appropriate filter response curves $S_{x_1}(\lambda)$ and $S_{x_2}(\lambda)$. Equation 4.2 is applied at all redshift intervals Δz within the specified z-range defining the color involved. The calibration constant C was fixed using equation 4.3 and data from table 3. The following normalised equations have been used in computing the $B-R$, $R-K$ and $B-V$ colors (from eqn.4.2):

$$B-R = 2.5log\left[\frac{F_R}{F_B}\right] + 1.448$$

$$R-K = 2.5log\left[\frac{F_K}{F_R}\right] + 4.051$$

$$B-V = 2.5log\left[\frac{F_V}{F_B}\right] + 0.647$$

Results of output for various colors as a function of z are shown in table 3. Plots of $B-R$, $R-K$ and $B-V$ vs z are shown in figure 18. The rapid variation in color with z for the $B-V$ plot is a consequence of the various emission lines in the Ly-α region entering and leaving the B and V passbands. In particular, all three plots in figure 18 show a gradual reddening or an abrupt increase in color towards higher redshifts, this again is due to the large relative flux from the Ly-α region entering the last bandpass of a specific color as the composite is redshifted. The $R-K$ vs z plot shows a "redder behaviour" at low redshifts than the other plots. This is due to a greater relative flux entering the K band at $z=0$ as seen from the composite of figure 17.

These predicted color vs z plots will be particularly useful later on when they are compared with the observed colors of quasars of different redshift. They will provide a useful diagnostic for indicating the existence of any excessive reddening in observed sources-most importantly in our selected empty fields whose nature is to determined.

Redshift	U-B	B-V	B-R	B-K
0.0	-.200	.025	1.487	6.646
0.1	-.233	.029	1.370	6.467
0.2	-.219	.037	1.315	6.270
0.3	-.226	.003	1.317	6.097
0.4	-.171	-.013	1.311	5.920
0.5	-.113	.012	1.307	5.777
0.6	-.081	.041	1.313	5.656
0.7	-.084	.053	1.331	5.556
0.8	-.145	.119	1.375	5.481
0.9	-.192	.164	1.415	5.405
1.0	-.199	.165	1.446	5.319
1.1	-.138	.128	1.438	5.198
1.2	-.140	.105	1.449	5.112
1.3	-.151	.077	1.462	5.035
1.4	-.145	.062	1.471	4.963
1.5	-.076	.047	1.457	4.876
1.6	.000	.051	1.435	4.790
1.7	-.023	.112	1.451	4.745
1.8	-.051	.139	1.460	4.698
1.9	-.087	.162	1.489	4.668
2.0	-.083	.174	1.519	4.638
2.1	-.006	.177	1.529	4.590
2.2	.195	.165	1.501	4.507
2.3	.403	.187	1.493	4.449
2.4	.469	.227	1.540	4.451
2.5	.476	.261	1.604	4.481
2.6	.484	.291	1.673	4.522
2.7	.531	.326	1.746	4.579
2.8	.616	.356	1.813	4.654
2.9	.637	.406	1.889	4.757
3.0	.690	.495	1.962	4.864
3.1	.740	.633	2.046	4.971
3.2	.761	.760	2.133	5.081
3.3	.810	.852	2.227	5.203
3.4	.830	.912	2.335	5.333
3.5	.943	.971	2.460	5.475
3.6	.992	.982	2.588	5.610

Table 3: Quasar colors as a function of redshift using the composite spectrum of fig.17.

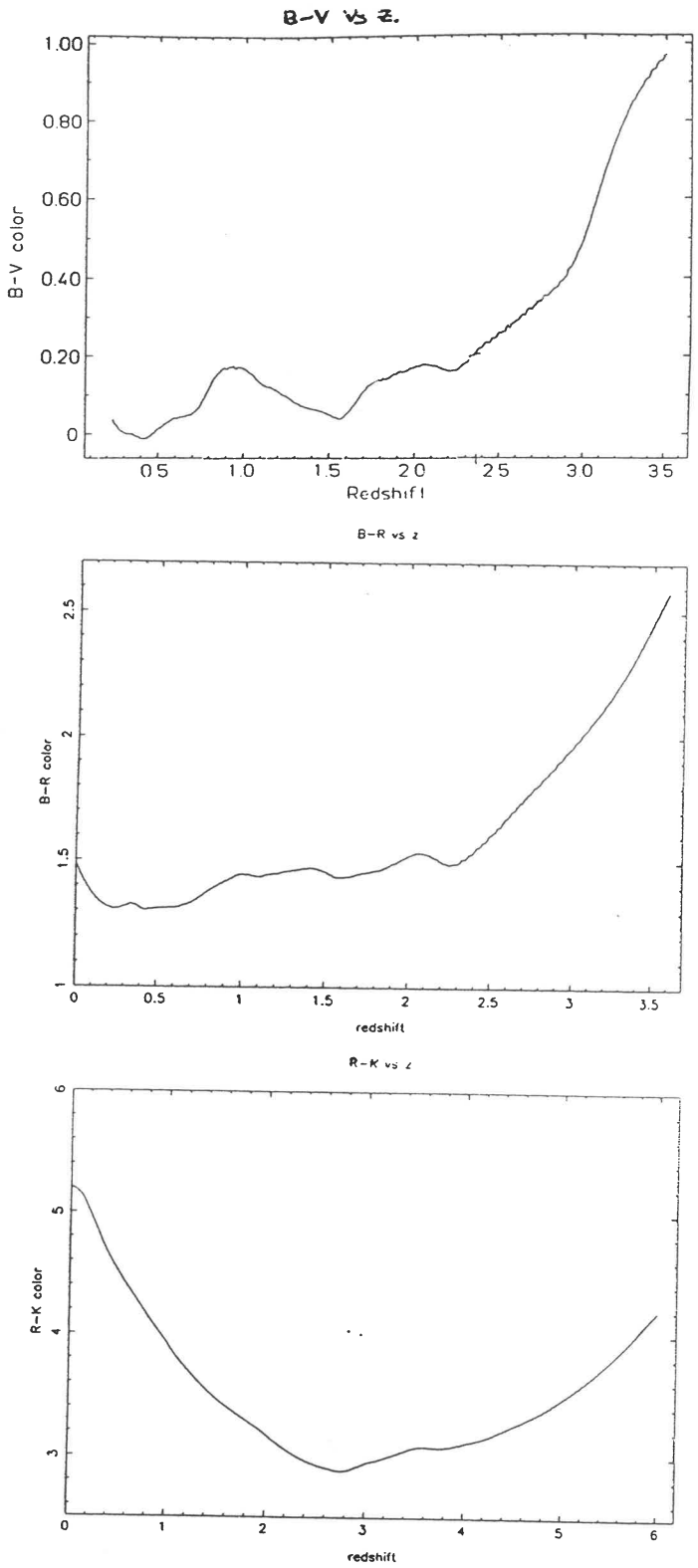

Figure 18: Predicted relationships between quasar colors and redshift using the Francis + McDowell rest frame composite.

5 Observations and Quasar samples

5.1 The observations.

Empty fields for infrared imaging were taken from a complete sample compiled by Savage et al.(1990). This sample was initially selected from the Parkes 2.7GHz survey (Bolton et al.1979) and was comprised of 403 flat spectrum radio sources with flux densities > 0.5 Jy. The aim of their study was to determine in an unbiased manner the space distribution of quasars over a large region of sky. Based on positional coincidence alone, Savage et al. obtained optical identifications for 87% of their sample to the 22 B_J mag limit of the UK-Schmidt sky survey plates and to the 24.0 R mag limit of CCD frames obtained with the AAT. 51 sources have been classified as empty fields to the limit of the Schmidt plates, and of these, about 20 have missing R-band images. We have considered the possiblity of identifying some of these sources at infrared wavelengths, which may provide a possible insight into the nature of their obscuration.

Observations were made during two nights at the Anglo-Australian Telescope in June 1993. Our selected empty fields have been successfully identified in the infrared using the K_N filter (centered at 2.15μm with a bandwidth 0.3μm). Infrared imaging was performed using IRIS-an infrared camera mounted at the $f/15$ Cassegrain focus of the 3.9-m telescope. The infrared detector consists of an array of 128×128 pixels, each 60μm square and each capable of reaching an image scale of 0.27 arcsec. Our IR images were made to correspond to an image scale of about 0.61 arcsec per pixel. To exclude extinction effects from dust in the galactic plane, all sources observed had galactic latitudes $|b| > 20°$. The method used to observe and verify the positions of our identified sources was as follows:

1. A set of 15 sources, comprising of eleven empty fields and previously identified quasars of known redshift taken from the sample of Savage et al. were succesfully imaged in the infrared by centering the measurement aperture on the radio positions. Exposures were of length 1200 sec. of which enabled us to identify sources up to a magnitude of $K_N \sim 20.0$ (see table 4).

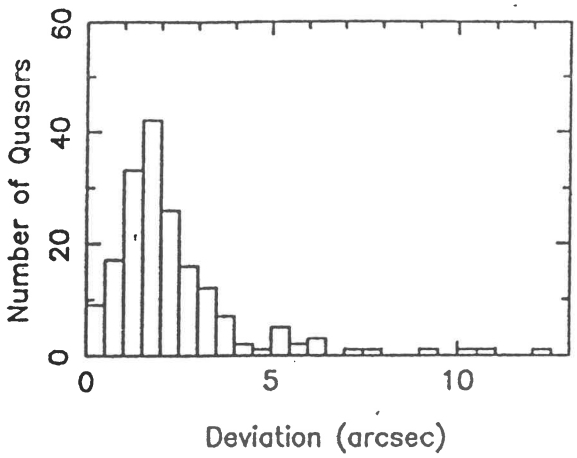

Figure 19: Deviation between COSMOS positions and other accurately available positions. (L. Kedziora-Chudczer MSc. Thesis, 1992).

2. Identifications were based on positional coincidence with the radio position. Ten out of eleven empty fields observed in the K_N-band were all detected to within an accuracy of 1.5 arcsec from the radio position. We were confident in the position of the correct identification due to the fact that all our sources were associated with "compact" radio components-a property of most flat spectrum sources. Their radio positions are much more accurately defined than the extended sources typical of galaxies.

3. The field of view covered by the IR camera (~80 arcsec) was sufficiently large to contain several stars which were also visible on the Schmidt-COSMOS plates. These plates are actually sky maps containing sources to a magnitude limit B_J ~22. Each CCD-IR frame was matched with its corresponding COSMOS plate which contained most objects in the field of our suspected IR image. This procedure provided us with a set of standard stars of known position which were used to perform the astrometry-a task for accurately determining positional uncertainties in our detected sources.

4. Astrometry was performed using the "Astrom package" from the Starlink project. The procedure basically involved using two or more bright stars as standards to perform a required rotation and/or translation of the coordinate IR frame to match the appropriate region of the COSMOS field. Typical deviations between COSMOS positions with those measured from optical or radio surveys are shown in figure 19. We can see that deviations may be as great as 2 arcsec. Positional discrepancies of ≤ 2.5 arcsec were obtained for most sources after reperforming the final astrometry using the COSMOS data (see table 4).

5. IR frames of standard IR stars each of exposure 30 sec. were also taken throughout the observing session. These will aid in the calibration

of the photometry to be dicussed in section 5.3.

Note that four of our identified empty fields were not associated with any COSMOS listing. The astrometry for these sources was somewhat more involved since it relied on using uncertainties derived from R-band positions of reference stars and then testing for positional coincidence of the radio and IR image. The digitised HST Guide Star catalogue was used to match reference stars in R fields for confirming the accuracy of coordinate positions.

Positive R-band detections have been previously obtained for about five of our selected empty fields. Webster (1992-93) (unpublished data), obtained R-band frames for all sources in our sample from observations with the 2.3 metre and the AAT at Siding Spring Observatory to a limiting magnitude of R=24. R-band frames have also been obtained by Peterson & Jaucey (1987-unpublished data). CCD frames of these sources have as yet not been fully reduced so that photometry be performed to determine true R-band magnitudes. R magnitudes are at present unavailable, though we intend to image all of our empty fields in R in further observing runs at the 2.3 metre telescope.

5.2 Results.

The table on the next page gives a summary of our identified sources in the IR. Note all sources have radio fluxes > 0.5Jy corresponding to 2.7GHz and all are of the flat spectrum type ($\alpha_{1.4-2.7GHz} < 0.5$). The layout in columns is as follows: (1), The Parkes source number; (2), Coordinates of the radio position (expected position of IR image) for epoch J2000 from the Parkes catalog (hr, min, sec for RA and °, ′, ″ for Dec.); (3), source IDs from the Parkes catalog-previously observed quasars (Q) of known redshift (in brackets) and empty fields (EF); (4), The position of our IR identification (only given in last units: s in R.A. and ″ in Dec. The larger units are as given in column 2); (5), Difference between radio and IR position from astrometry; (6), Calculated $K_N(2.15\mu\text{m})$-band magnitudes from photometry (see section 5.3); (7), Error in K_N magnitudes from photometry; (8), B_J magnitudes to the limit of the UK-Schmidt plates ($B_J = 22$). The source B2224+006 has been identified as a faint stellar object whose redshift is unknown, its quasar identification is uncertain.

Table 4: Observed sources.

(1) SOURCE	(2) radio position (J2000) R.A.	Dec.	(3) ID	(4) IR position R.A.	Dec.	(5) pos.diff. (arcsec)	(6) K	(7) K	(8) B
B1430-155	14 33 21.47	-15 48 44.6	EF	21.30	45.97	2.15	18.075	0.122	>22
B1511-210	15 13 56.98	-21 14 57.4	EF	56.92	57.93	0.58	16.954	0.033	>22
B1535+004	15 38 16.00	+00 19 05.0	EF	15.84	5.23	0.90	19.540	0.428	>22
B1557+032	15 59 30.95	+03 04 47.7	EF*	30.99	48.78	2.60	17.111	0.045	>22
B1654-020	16 56 56.09	-02 06 49.7	EF	56.00	49.80	2.30	18.261	0.122	>22
B1732+094	17 34 58.38	+09 26 58.3	EF*	58.37	58.48	0.89	16.276	0.018	>22
B2047+098	20 49 45.86	+10 03 14.4	EF*	45.27	9.72	5.20(?)	18.888	0.165	>22
B2056-369	20 59 41.55	-36 45 54.5	EF	41.54	54.99	0.49	18.159	0.072	>22
B2149+056	21 51 37.87	+05 52 12.9	EF*	37.91	11.60	2.11	14.901	0.017	>22
B2304-230	23 07 38.66	-22 47 53.1	EF	38.65	51.80	1.80	17.445	0.057	>22
B1706+006	17 08 44.62	+00 35 09.4	EF	44.24	10.78	1.09	15.310	0.010	>22
B2000-330	20 03 24.12	-32 51 44.5	Q(3.78)	24.06	44.54	0.85	14.911	0.006	19.560
B2126-158	21 29 12.17	-15 38 41.1	Q(3.275)	12.07	41.6	0.88	14.046	0.004	16.565
B2215+020	22 17 48.24	+02 20 10.7	Q(3.55)	48.24	10.7	0	16.652	0.028	21.5
B2224+006	22 24 13.10	+00 36 52.0	Q(?)	13.1	52.0	0	14.320	0.005	22.500

* No COSMOS fields available for these sources.

5.3 Photometry.

The detected infrared sources on our IR frames (eg. figure 20) are not representative of the true apparent flux that they emit. Each IR image is contaminated by a background sky flux contributed by stars and other sources within the same field. Exposure times, system properties and seeing conditions are also effects that contribute to the "raw" flux as interpreted from a CCD image. These effects are needed to be corrected for if we are to extract true magnitudes for our sources (as listed in column 6 of table 4). This procedure is commonly referred to as photometry.

The apphot task in the IRAF package was used to subtract the effect of sky noise. The procedure basically involves defining an annular aperture around the suspected source which represents the region of sky to be subtracted. This was particularly simple since our sources were not in heavily crowded stellar fields. Output from the program resulted in a sky corrected K_N-magnitude for each suspected qusasar: $(M_{sc})_{quasar}$.

Properties characteristic of the system (detector) used together with the seeing conditions such as atmospheric effects must also be taken into account. These effects can be determined by use of the following standard stars of known "true" K_N-magnitude $(M_t)_{standard}$, which were photographed at regular intervals throughout the observing session:

source :	$(M_t)_{standard}$	$(M_{sc})_{standard}$
HD159402	8.140	11.308
HD201916	7.786	10.946
HD88449	8.223	11.666

The exposure time used on each of these standard stars was 30 sec.

Denoting sky corrected K_N-magnitudes for each of the standard stars by $(M_{sc})_{standard}$, the magnitude factor responsible for both system and seeing effects is then the difference :

$$(M_t)_{standard} - (M_{sc})_{standard} = C \tag{5.1}$$

Finding C for each of the three standard stars and taking the average (C_{av}), we can then represent the true K_N-magnitude for each of our imaged quasars

or empty fields by

$$(M_t)_{quasar} = (M_{sc})_{quasar} + C_{av} + \Delta M_{Exp.} \tag{5.2}$$

where $\Delta M_{Exp.}$ represents a magnitude factor due to a difference in exposure times used for the quasars and standard stars. Since exposures for the quasar and standard frames were of length 1200 sec. and 30 sec. respectively, the total flux received by the CCD detector is a factor of 40 greater when quasar frames were taken. Thus in magnitudes, the corresponding factor is

$$\Delta M_{Exp.} = 2.5log(40) = 4.00515.$$

In our case, the system and seeing effects parameter (C_{av}) took the value -3.257, so that overall we have

$$(M_t)_{quasar} = (M_{sc})_{quasar} + 0.748 \tag{5.3}$$

The true K_N-magnitudes as listed in column 6 of table 4 were calculated using 5.3 once sky corrected magnitudes $(M_{sc})_{quasar}$ were found from the IRAF package. Uncertainties in column 7 are only due to the sky subtraction process and were taken directly from the output given by the apphot program.

Figure 20(b) (next page) shows a typical CCD frame taken of the empty field B1654-020 (see table 4). (a) Shows the corresponding region of the UK-Scmidt plate or COSMOS field as would be expected from a B_J frame to a magnitude limit of $B_J = 22$, the cursor marks the radio position of the suspected IR image. (b) shows the same region imaged in the K_N-band. Also shown in (a) are some labelled reference stars used for the astrometry, some of them also appear in the K_N-band image. The cross in the IR frame of fig. (b) indicates the radio position and a distinct image is noticed (labelled by arrow) which does not appear in the COSMOS field of (a). This is believed to represent the true IR image as confirmed within positional errors from the astrometry. The pixel dimensions of this frame as shown measure 155 $\times$ 161. The pixel coordinates of the radio position and suspected IR image are respectively 55,90 and 59,91. Since each pixel has an image scale of 0.615", the positonal difference is about 2.3" which is also indicated in column 5 of table 4.

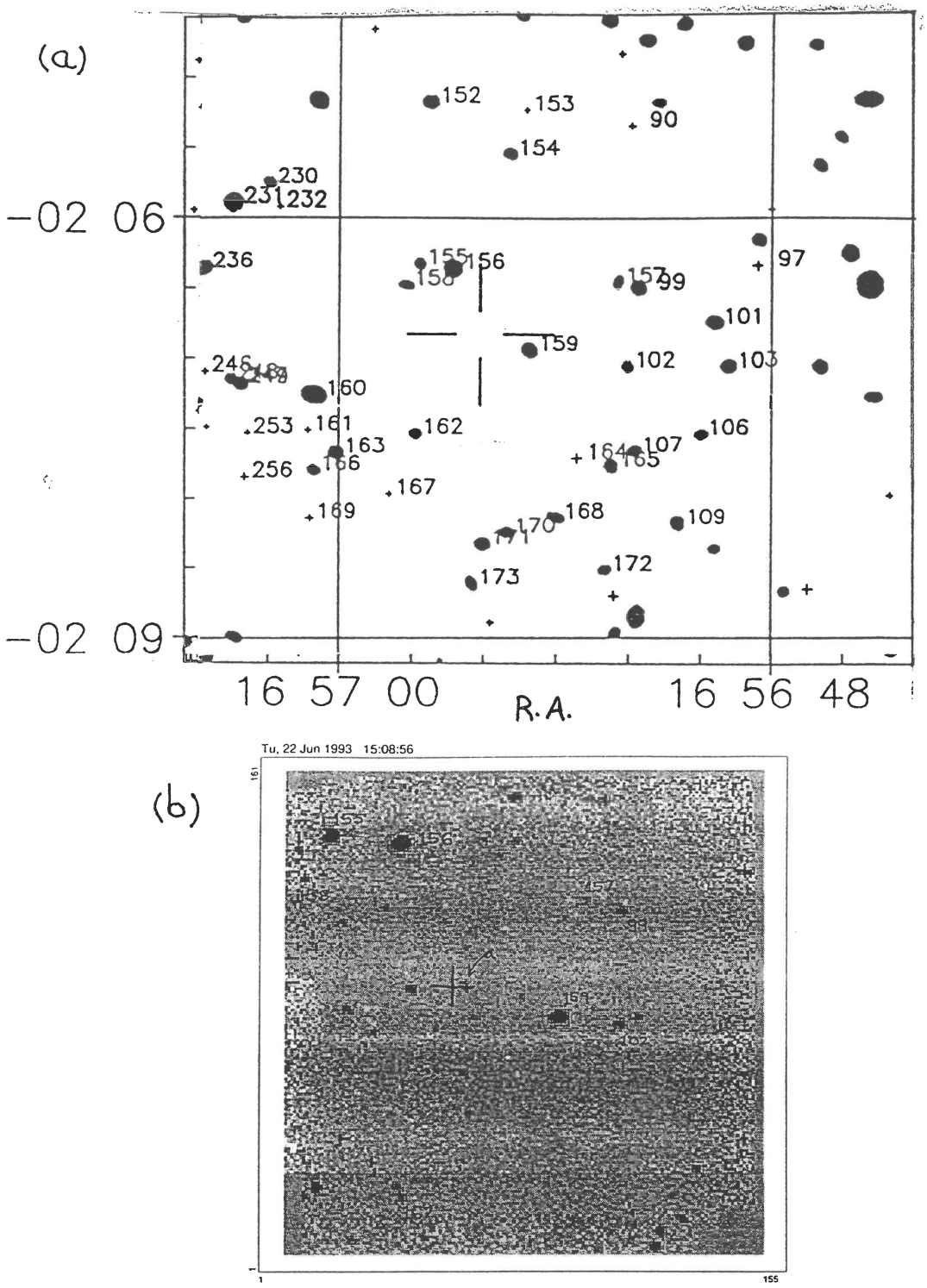

Figure 20: (a) COSMOS field to B_J=22 corresponding to the empty field B1654-020 (see table 4) with the radio position indicated. (b) The CCD-IR frame whose scale is larger than the COSMOS map, reference stars have been labelled accordingly. The suspected image is labelled by the letter a and the cross is its expected positon-the radio position.

5.4 Samples from other datasets.

In this section I will list some previously identified quasars and empty fields for use in conjunction with the observed sources of table 4 for analysis in the next section. Most of the data to follow is selected on the basis of flat and compact radio spectra, though I have also included a few sources which have moderately steeper spectra ($\alpha > 0.5$). Since radio selected sources are unbiased with regards to observations made at infrared wavelengths and hence reddening effects, steep spectrum sources have also been included. Observations having yielded positive IR identifications have only been considered. Furthermore, based on the diverse range of radio flux limits at which observations have been made, sources with a variety of radio fluxes have also been chosen.

Table 5 on the following page is a list of previously identified quasars, whose redshifts (z) have been determined. This list was selected from a complete sample of Parkes radio sources compiled by Dunlop et al. (1989). From their sample of 178 sources, 41 are flat spectrum sources and of these, 73% have been identified with quasars. Their $B(0.44\mu\text{m})$, $R(0.7\mu\text{m})$ and $K(2.2\mu\text{m})$ observations have been converted into the colors shown. The radio flux limit for their sample is $S_{2.7GHz} > 0.1\text{Jy}$. This has led me to define two categories for the selected quasars based on radio flux: those with $S_{2.7GHz} > 0.5\text{Jy}$ (table (a)) and those with $S_{2.7GHz} < 0.5\text{Jy}$ (table (b)). The sources listed have been selected on the basis of their quasar identification as confirmed from spectroscopic studies by Dunlop et al. (1989). Only quasars for which K-band magnitudes had been determined are listed.

The reason for selecting sources from this particular sample is that it provides an extensive optical and infrared study of radio sources in the Parkes selected regions for which colours have been determined. This has enabled me to select on radio properties alone-mostly the flat spectrum behaviour that is apparent in most quasars. The inclusion of some steeper spectrum sources is to provide a broader redshift range of identified quasars. The third column in table 5 lists the mean spectral index within the frequency range 1.4-2.7GHz.

The second sample consists of six empty fields taken from Rieke et al. (1979) (see section 3.3). These sources (see table 6) are associated with flat

spectrum radio sources which had been missed in the optical to magnitude $V(0.55\mu m) = 19.5$. The $B - K$ colors listed were computed from V and K fluxes as measured by Rieke et al. B magnitudes were determined from given V magnitudes using the simple transformation $B = V + 0.3$ which holds for most observed quasars.

Table 5: Quasars from Dunlop et al. (1989).
(a) Sources with S(2.7GHz)>0.5Jy:

SOURCE	S(2.7GHz)	Spect.ind.	z	B-R	R-K	B-K
B0003-003	2.410	0.72	1.037	0.90	2.80	3.70
B0038-019	0.650	1.22	1.679	-0.80	2.80	2.00
B0056-001	1.960	0.49	0.717	0.10	1.64	1.74
B0105-008	0.730	0.26	0.318	0.20	1.83	2.03
B0222-008	0.660	0.79	0.687	1.30	2.65	3.95
B0233-025	0.580	0.78	1.321	0.10	2.20	2.30
B1351-018	1.000	-0.08	3.709	1.60	2.04	3.64
B2154-184	1.108	1.17	0.668	0.37	4.23	4.60
B2154-183	1.001	0.79	1.423	-0.81	4.95	4.14
B2203-188	5.200	0.32	0.618	0.90	2.45	3.35
(b) Sources with S(2.7GHz)<0.5Jy:						
B0007+016	0.160	0.84	2.900	0.90	3.14	4.04
B0045-000	0.110	0.24	1.536	0.10	1.49	1.59
B0223+012	0.240	0.76	1.369	1.10	0.66	1.76
B0235+023	0.293	0.72	0.209	0.60	3.66	4.26
B0236-015	0.147	1.08	1.794	-0.10	2.26	2.16
B0237-027	0.400	-0.41	1.116	0.60	0.47	1.07
B0240-021	0.122	0.95	0.617	0.82	2.84	3.66
B0242+009	0.164	0.91	1.520	1.40	2.04	3.44
B1157+014	0.143	0.45	1.986	0.87	2.41	3.28
B1158+007	0.257	0.26	1.367	0.61	1.21	1.82
B1215-033	0.108	0.88	0.184	1.97	3.55	5.52
B1348+007	0.132	0.37	2.084	0.52	5.28	5.80
B2153-204	0.220	0.20	1.310	0.60	1.17	1.77
B2158-206	0.235	0.67	0.370	-0.10	2.83	2.73
B2203-615	0.158	-0.19	0.577	-0.20	2.81	2.61
B2214-206	0.125	0.97	2.316	0.44	4.09	4.53
B2357-007	0.101	-0.13	1.107	1.38	3.15	4.53

Table 6: Empty fields from Rieke et al. (1979).

SOURCE	B-K
0026+34	5.45
0406+121	5.05
0602+67	-
1413+135	5.805
2255+418	5.798
0348+049	5.227

6 Analysis

6.1 Testing the Hypothesis.

Radio observations have provided us with complete and unbiased quasar samples as the statistics for flat-spectrum sources show. More than $\sim 72\%$ of flat spectrum radio sources have been associated with quasars.

This project was initially motivated by the presence of sources in the complete flat spectrum radio sample of Savage et al. (1991) which had missed detection in the B_j band to magnitude 22. Since a majority of these sources had also missing R-band images, it was proposed that such sources had missed optical detection because they were "exceedingly" red in colour, possibly due to dust. The prediction was to look for such sources in the infrared. With success, we are now faced with the primary task of interpreting the nature of the observed reddening in our radio selected quasars.

If obscuration due to dust is present, then quasar selection based on IR observations will be greatly biased by excessive reddening effects. The infrared offers little chance in providing a strong selective property that may aid in quasar identification. Besides flat radio spectra, further evidence to suggest that our imaged empty fields in table 4 are strong quasar candidates is that all IR and some R band images are very stellar in appearence.

The suspected quasar sources in table 4 are ideal for testing whether dust be responsible for their obscuration. Such dust may be within intervening galaxies, uniformly distributed along the line of sight, or associated with the quasar itself-ie within a surrounding torus. These sources may give a direct hint as to how much dust there really is distributed throughout the universe which may be obscuring distant sources and hence giving us a somewhat different interpretation of quasar evolution and cosmology. It is important to note that the imaged empty fields in table 4 may also represent quasars which are at very large redshifts, they may also at the same time be obscured by various amounts of dust.

In this section I will investigate the nature of our identified empty fields using their observed colours. Their detection in the IR (K-band) offers a valuable opportunity in testing whether the observed reddening can be attributed to high redshift, dust or both. The former case will be investigated

via use of the predicted colors from the K-correction discussed earlier. In other words are these sources redder than what they're predicted to be assuming a redshifted standard composite quasar spectrum? Can the reddening be explained in terms of a redshifted Ly-α continuum alone? Comparisons with previously identified optical quasars will be made to determine if there is in fact an excess reddening in our imaged empty fields which may provide strong evidence for a dust hypothesis. The table below shows the observed $B - K$ colours for our sources computed from table 4. Only lower limits on colours are available for the empty fields, this is a consequence of the B_j magnitude limit to which they have missed detection (see table 4).

SOURCE:	ID	$B_j - K_N$:
B1430-155	EF	> 3.925
B1511-210	EF	> 5.046
B1535+004	EF	> 2.46
B1557+032	EF	> 4.888
B1654-020	EF	> 3.739
B1732+094	EF	> 5.724
B2047+098	EF	> 3.112
B2056-369	EF	> 3.841
B2149+056	EF	> 7.099
B2304-230	EF	> 4.555
B1706+006	EF	> 6.69
B2000-330	Q	4.649
B2126-158	Q	2.519
B2215+020	Q	4.84
B2224+006	Q	8.18

Table 7: $B_j - K_N$ colours of observed sources.

6.2 Comparison with other Datasets.

The histograms on the following page give an indication that our identified empty fields of table 4 are on average "redder" than the optically identified quasars of the Dunlop et al. sample (table 5). Only flat spectrum sources from the Dunlop sample have been plotted (fig. 21(b)), since our empty fields (fig. 21(a)) were selected from a flat spectrum population only. The median reddening in magnitudes for our empty field sample and the Dunlop sample is respectively > 4.2 and 2.8 in $B - K$ colour. Our empty fields are on average > 1.4 magnitudes redder in $B - K$ colour than the optical flat spectrum quasars of table 5. Results of a Kolmogorov test indicate that the chance that the two samples are considered as the same population is 0.61%, this is highly significant, being well below the significance level of 5%. This provides strong evidence to suggest that the empty fields have missed detection because of excessive reddening effects.

It is important to note that we only have a lower limit on the reddening excess for a particular empty field. The difficulty is in determining the "true" amount by which our empty fields are reddened as compared to previously identified optical qausars. This true reddening excess may then be used to determine whether it is sufficient to explain why the empty fields have missed detection to at least $B = 22$. The nature of the reddening ie-"dust" or "high" redshift may then also be accounted for. At present, we can only constrain models for the reddening according to the available lower limits in table 7.

As noticed from our sample of sources in table 7, all sources show a spread in $B - K$ colour, indicating that they are not all reddenned by the same amount. This is the same for the Dunlop et al. sample in figure 21(b), the variance in $B-K$ for each histogram is very similar. Since the Dunlop sample is comprised of quasars with B-band identifications to magnitude 21, their sample is expected to represent a "dust free" population. In other words, the fact that any B-band flux is observed from them at all, suggests that their optical emission is less likely to be affected by dust. The presence of dust is generally associated with extinction at bluer or shorter wavelengths. The spread in optical-infrared colour in the Dunlop sample can be attributed to the K-correction alone-ie a varying spectral flux entering different bandpasses as the continuum is redshifted. This will be further investigated in the next section.

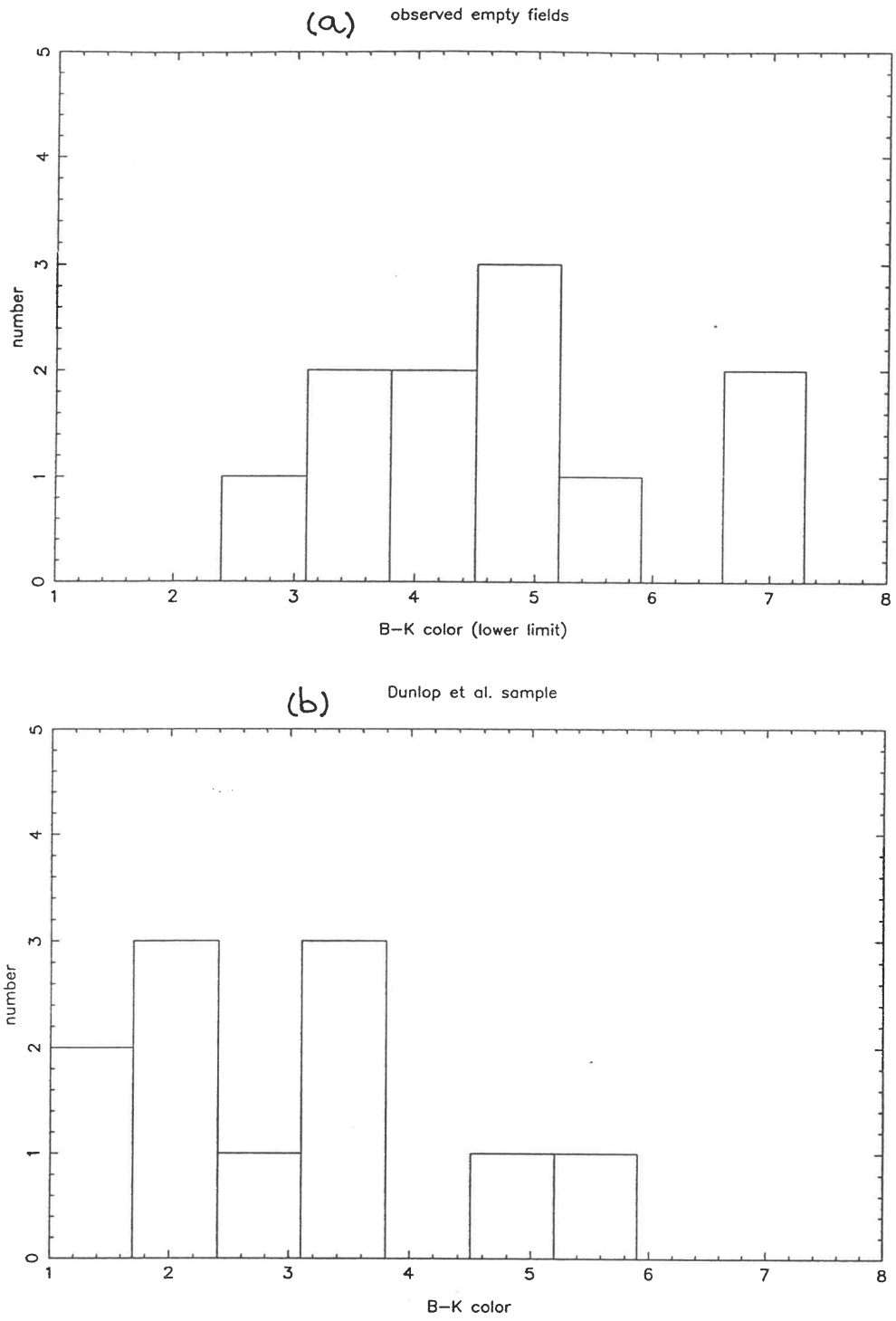

Figure 21: Histograms showing the distribution in $B - K$ colours in our selected empty fields (fig. (a)) and optically identified quasars (fig. (b)) from the Dunlop et al. sample (1989)-see table 5.

Again, since lower limits in $B-K$ are only known in our observed sample, the spread in $B-K$ may actually be greater, this is expected if each source is affected by different distributions or amounts of dust either intrinsically or along the line of sight. Otherwise, all of the empty fields may actually represent a high redshift quasar sample, which is obscured and reddened in a systematic way. The four identified quasars in table 4 which were also relatively bright in the IR are also comparatively reddened as indicated by their $B-K$ colours. In particular, the suspected quasar B2224+006, although being associated with a faint optical starlike image at $B = 22.5$, is in fact the reddest source in our sample. Extinction due to dust in this source may be as great as 7 magnitudes in the B band. The empty fields may represent sources which also suffer extinction due to dust by at least the same amount. The difficulty with these sources is that their redshifts are not known, preventing us from isolating the reddening associated with the K-correction.

The $B-R$ and $R-K$ colours of quasars in the Dunlop et al. sample as listed in table 5, may also be compared with those of our empty fields. Though R-band magnitudes are as yet to be determined for our empty field sample. At present we know that some of the empty fields may have missed identification to $R = 24$. From table 5, it is noticed that almost all sources-in particular the flat spectrum sources ($\alpha < 0.5$) have $B-K$ colours which are greater than their respective $R-K$ colours. This suggests that if we consider our empty fields to be part of the same population of optically identified quasars as in table 5, then a new lower limit on the B manitudes for our empty fileds may be $B > 24$. This result only holds on the assumption that the empty fields be represented as an "optically faint" quasar population where the relation $B-K > R-K$ is expected to hold. This relation may be directly explained via a spectral property of the quasar, it may be due to a larger relative flux that remains within the B bandpass for a wide range of redshifts as compared with that in the R bandpass. This is evident in the redshifted composite spectra of figure 15.

With a new lower limit of $B > 24$ for only those empty fields in table 7 which have missing R-band images to $R = 24$, the lower limits in $B-K$ colours for these sources may actually be redder by a further two magnitudes. Extinction by dust may then further redden these colours by an amount that can only be deduced from the amount and distribution of dust involved. Dust is known only to remove flux in the B-bandpass-ie through scattering and/or absorption of "blue" wavelength photons. Also, if dust is intrinsic

to a continuum source, then it may be heated by lower frequency radiation and contribute a flux in the infrared (K-band) through thermal reprocessing. The net effect is then an overall increase or reddening in $B-K$ colour of the empty fields in table 7. The Rieke et al. sample of empty fields in table 6, have also $B-K$ colours which are redder than the median reddening in $B-K$ colour from table 5 as well as table 7. Their relatively large $B-K$ colours indicate that excessive reddening due to dust may also be present.

6.3 Colour vs. Redshift.

In this section, I will investgate whether the behaviour of the colours of previously identified optical quasars (from table 5) with redshift follows with the predictions shown in the colour vs. z plots of figure 18. The predicted colour vs. z plots will be used to determine whether the $B-K$ colours of our sources in table 7 can be attributed to the redshifting of certain spectral properties.

On the following page I have plotted data from table 5 with the predicted colour vs. z curves. I have also included the steep spectrum sources (open circles) for comparison, which being identified as quasars from stellar images and spectroscopic data, have been used to test the expected relationship between colours and redshift as predicted from the redshifted composite of figure 17. Only sources whose redshifts and colours fall within the ranges of the colour vs. z curves have been plotted and three flat spectrum sources (filled circles) fall within such ranges. These plots suffer from the lack of high redshift data, which is unavailable from present quasar samples in which quasars have been selected by radio means and at the same time identified in the infrared. We hope to obtain such data in the near future using the flat spectrum radio source sample of Savage et al. (1990).

It is expected that optically identified quasars should follow the theoretical prediction quite well, though in some cases, this is not the case. The $R-K$ data as plotted in figure 22(a) shows considerable scatter about the predicted curve. Such a scatter may be attributed to large intrinsic variations between the spectra of the quasars in the Dunlop et al. sample. In other words the continuum properties of quasars in this sample may show very little overlap. Such a scatter of 0.5-2 magnitudes from the theoretical may be due to extrinsic effects such as dust. Various amounts and

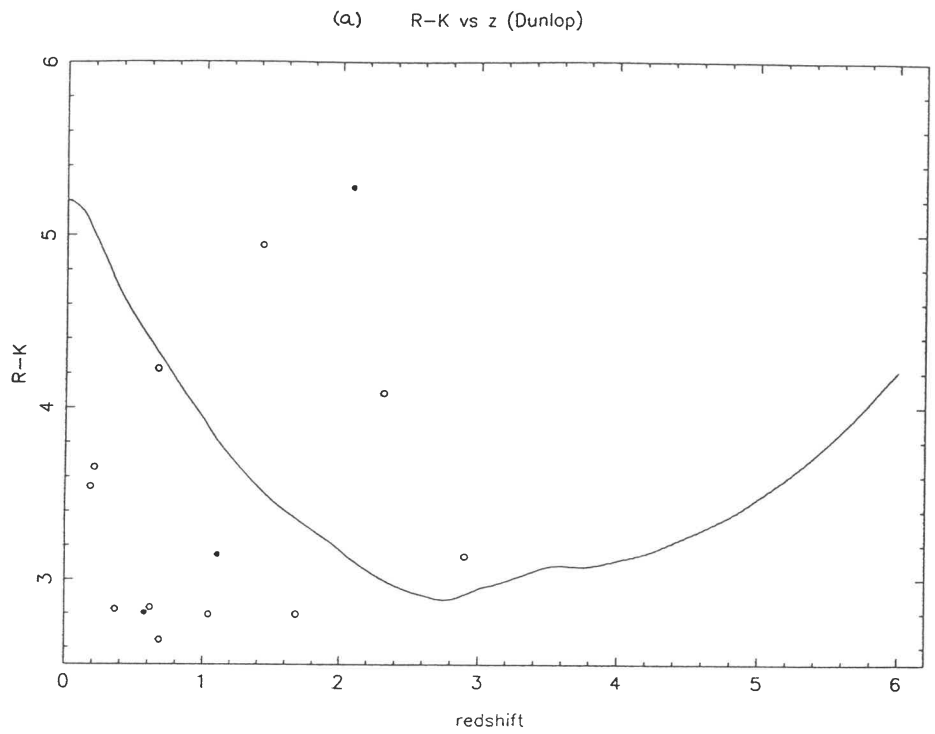

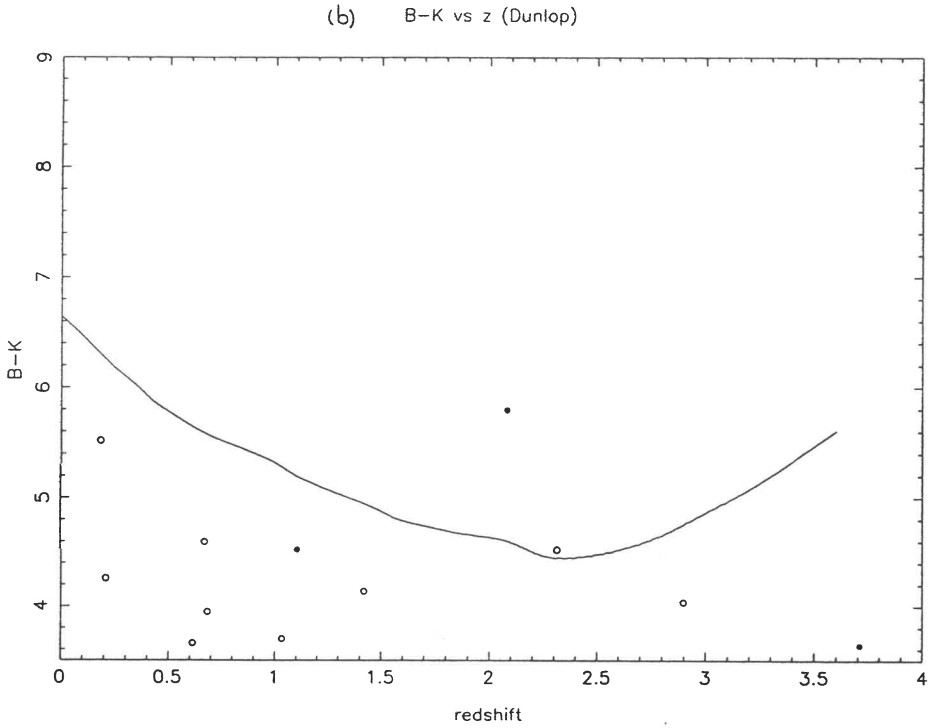

Figure 22: Data from the Dunlop et al. sample (table 5): filled circles-flat spectrum sources and open circles-steep spectrum sources. The curve represents the theoretical prediction calculated from the composite of figure 17.(a)$R-K$ vs z, (b)$B-K$ vs z, and (next page) (c)$B-R$ vs z.

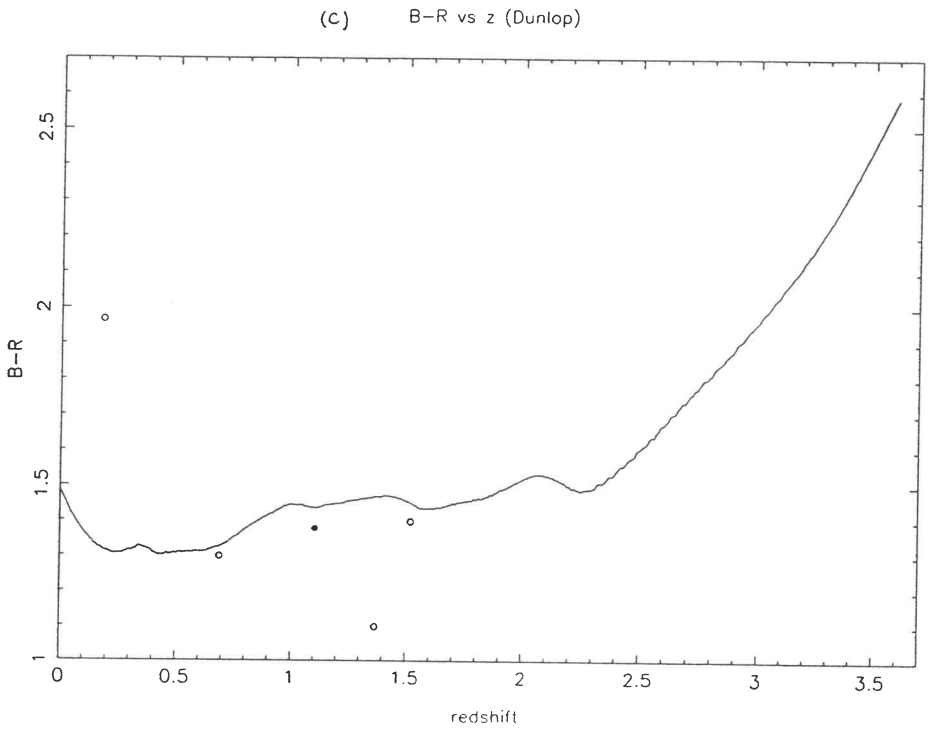
(c) B−R vs z (Dunlop)
B−R
redshift
1
1.5
2
2.5
0
0.5
1
1.5
2
2.5
3
3.5

distributions of dust at different redshifts can have an effect of reddening the quasar colours in a sample by random amounts therefore introducing a scatter.

The data points plotted in figure 22(b) appear to be bluer than the predicted theoretical curve, this is not expected, though a larger quasar sample may give a more even distribution of points about the predicted curve. The $B-R$ vs. z prediction tends to show close agreement with the three plotted sources implying that $B-R$ colour may be least affected by dust. A larger sample of $B-R$ colours is required to support this statement.

Given a particular redshift, the corresponding quasar colour can be deduced from the predicted colour vs. z curve and vice versa. There is more of an uncertainty in the reverse procedure of determining a redshift from a colour as is noticed from the large deviations between theoretical z values using the curve and measured z values from spectroscopy as listed in table 5. In fact, if there is no excess reddening in a particular source due to dust, then a colour vs. z curve may provide a very good distance indicator. This is not the case as is seen from the scatter using the Dunlop et al. sample in figure 22. Though the colour vs z plots may be useful in classifying the nature of the reddening in some quasar sources and possibly empty fields.

The redshifts of the two flat spectrum sources in the $B-K$ vs z plot were deduced from emission line spectroscopy and dust can never bias such a spectroscopic determination of redshift. Therefore for the flat spectrum source in the upper part of the plot in figure 22(b), its expected $B-K$ colour given that $z=2.084$ is about 4.6. Thus this source is observed to be ~ 1.2 redder. If the empty fields of table 7 are corrected for such amounts of extinction, then $B-K$ colours for some of the empty fields (especially for those with $R>24$-hence $B>24$) may actually still be quite red.

The problem is deducing how much reddening excess exists in the empty fields above that introduced by the K-correction that can be attributed to dust. At a particular redshift, there will be reddening at least due to the K-correction. Given a particular $B-K$ or $R-K$ colour, the plots in figures 22(a) and (b) introduce a difficulty in discriminating between high and low redshift sources. This is due to the parabolic shape in the theoretical curves- a consequence of the composite spectrum used (figure 17). At low redshifts, the K-band flux dominates and at large redshifts, the flux in the Ly-α region will dominate once the K-band flux is redshifted out of the K-band.

Since we only have lower limits in $B-K$ colours for our empty fields, it is

then only possible to place an upper and lower limit on the redshift expected. Table 8 shows the redshift limits in our empty field sources as deduced from the $B-K$ colours of table 8 and the $B-K$ vs z plot of figure 22(b). Only empty fields whose $B-K$ lower limit falls within the range of the plot are listed. The values at which the limits are based are due to the K-correction alone as predicted from the theoretical. Further reddening by dust will then tend to predict lower or higher redshifts according to the $B-K$ vs z plot. True redshifts can only be determined from such colour vs z plots if colours are corrected for dust extinction. Otherwise, extinction due to dust may leave the redshift of a quasar completely undetermined unless it is possible to deduce it spectroscopically in the infrared.

SOURCE:	limits:
B1511-210	$z < 1.35$ or $z > 3.1$
B1557+032	$z < 1.45$ or $z > 2.95$
B1732+094	$z < 0.55$ or $z > 3.6$
B2149+056	$z > 3.6$
B2304-230	$z < 2.1$ or $z > 2.6$
B1706+006	$z > 3.6$

Table 8: Redshift limits for some of the empty fields of table 7 predicted using the K-correction alone.

I believe that it is more probable that the redshifts of the empty fields satisfy the higher redshift lower limit case of table 8. The reason for this is that the three quasars B2000-330, B2126-158 and B2215+020 listed in table 4 which were also imaged in the infrared, have relatively large redshifts and observed colours comparable to those of the empty fields listed in table 7. Apart from B2126-158 which is quite blue in $B-K$ colour, the two other quasars have redshifts of 3.78 and 3.55 and respective colours 4.649 and 4.84. These points are off scale in the $B-K$ vs z plot. Though this indicates that the empty fields which are redder in $B-K$ colour may actually be quasars at high redshift, their colours being due to large amounts of intervening dust possibly associated with galaxies. They are at the same time sufficiently dimmed and hence obscured optically. A larger sample of optically faint

reddened quasars with large measured redshifts is required to support this statement. R.L.Webster (personal communication) has suggested that if a large proportion of "bluer" than expected quasars arise from high redshift surveys, then there is the possibilty that this may be due to "microlensing". This is lensing by small massive compact bodies which has a tendency of magnifying the blue flux. This somewhat complicates the dust hypothesis.

The empty fields may also be quasars which are at relatively low redshifts-ie with $z < 2$. The $B - K$ vs z curve in figure 22(b) predicts more reddening towards low redshifts than at higher redshift. It may be that the true $B - K$ colours of the empty fields in table 7 are much larger than the colour introduced by the K-correction at low redshifts. Reddening due to dust in intervening galaxies may be less probable but obscuration and reddening due to a dusty torus surrounding a quasar may be the case. An observational signature involving "dusty tori" associated with the empty fields is given in section 6.5.

The quasar B2126-158 in table 7 has been associated with a strong X-ray flux (Elvis et al. 1993). X-ray absorption towards this high redshift quasar has been detected and one suggestion has been attributed due to the presence of intervening damped Lyman-α absorbers. There is also a significant lack of reddening in this source as indicated by its by $B - K$ colour of 2.52. Considering its large redshift, this has been difficult to account for. Though it has been attributed to the fact of a sufficiently low dust to gas ratio in the damped Ly-α absorbers (Elvis et al. 1993).

As compared with optical-IR colours of previously identified optical quasars, the colours of our selected empty fields suggests that the presence of dust may be a significant factor in obscuring quasars. There may be more dust than what we expect distributed throughout the Universe. It is possible that such dust may lead to more than 8 magnitudes of extinction in the optical. This possibility has been overlooked in the past and we propose to further analyse optically obscured quasars to strengthen the dust hypothesis. Future prospects will be discussed in chapter 7.

6.4 Galactic Extinction?

The probability that obscuration by galactic dust in our own galaxy is responsible for the empty fields is quite small. All of the empty fields of table 7 are located at galactic latitudes $|b| > 20°$ and extinction due to dust may become significant towards the galactic plane. For $|b| < 10°$ it may be as great as 5.5 magnitudes in the B-band. The apparent B magnitude of a distant source at galactic latitude b would increase by an amount (Mihalas & Binney 1981)

$$\Delta m = 0.51 cosec(b)$$

due to galactic dust. For $|b| > 20°$ this law predicts an extinction in the B band of $\Delta m < 1.4$. It is unlikely that this magnitude extinction alone can be responsible in obscuring quasars to $B = 22$. The optical depth of galactic dust along our line of sight towards high galactic latitudes is relatively small as compared to that for an arrangment of intervening absorbers (Fall & Pei 1989). I beleive it may be difficult to account for the obscuration of quasars and a contribution of the large relative infrared flux observed in terms of galactic dust alone.

6.5 Intrinsic Obscuration-Dusty Tori?

Radio surveys involving quasars and active galaxies have shown that there exists a well defined relationship between radio structure and spectral index. Extended radio sources are usually associated with galaxies whose radio maps may show detailed structure such as double lobed components or diffuse emission. These sources tend to have steep power law spectra-ie spectral indices of $\alpha > 0.5$. Quasars on the other hand are associated with compact flat-spectrum radio cores, a majority of which have unresolved structure.

Included within the steep spectrum class are also active galaxies in which some tend to be associated with radio jets. Anisotropic emission such as radio jets has been generally modeled using accretion disks. Surrounding an accretion disk is the suspected dusty torus, axially symmetric with the radio emission.

With this knowledge, we have considered the possibility that that there may be some contribution to the obscuration of quasars from radiation partially obscured by an optically thick dusty torus. This may be a significant

factor, possibly accounting for most the empty fields. Although the empty fields are associated with flat radio spectra, it is predicted that their spectral indices are on average steeper than those for quasars that are visible optically. If extended radio emission is perpendicular to the plane of a torus, then a differential orientation with the line of sight of the torus axis would give rise to a variation in spectral index. A partial obscuration due to a dusty torus may be just enough to obscure and redden the central source but at the same time keep the spectral index relatively flat and hence radio source compact. The optically luminous quasars may then be sources in which the radio jets are actually directed more towards our line of sight and hence are less reddened and have a flatter spectral index.

To test this prediction, I have selected all of the flat spectrum sources from the Parkes catalogue which were identified into three classes: Empty fields, Quasars and BL-Lacs (see section 1.2) and the spectral index data was binned respectively. Results are shown in the histograms on the following page. As expected, figure (a) indicates that the empty fields have on average, steeper spectral indices than quasars and BL-Lacs. The median spectral indices are 0.17, -0.04 and -0.18 respectively. This provides a first hint for some intrinsic obscuration due to a dusty torus. There are alternative models other than dusty tori to account for the range of spectral indices and degree of obscuration involved. These involve the idea of decelerating plasmas through optically thick media (Cagonoff 1989), with the extended radio sources being associated with emission from optically thin regions. The three histograms indicate that BL-Lac type sources have the the flattest radio spectra. This supports the idea that such sources may be observed along their radio jet or nearly so and hence appear to be the most compact as confirmed from observation.

The Kolmogorov test was used to estimate the likelihood that any two data sets-ie quasars and empty fields or BL-Lacs and empty fields were drawn from the same flat spectrum population. In other words, how significant is the difference in any two distributions so that they can be considered as separate. Results indicate that the probability that the quasar and empty field samples are part of the same population is 0.43% and for the BL-Lac and empty field samples it is 0.38%. These results are well below the 5% significance level and hence are highly significant.

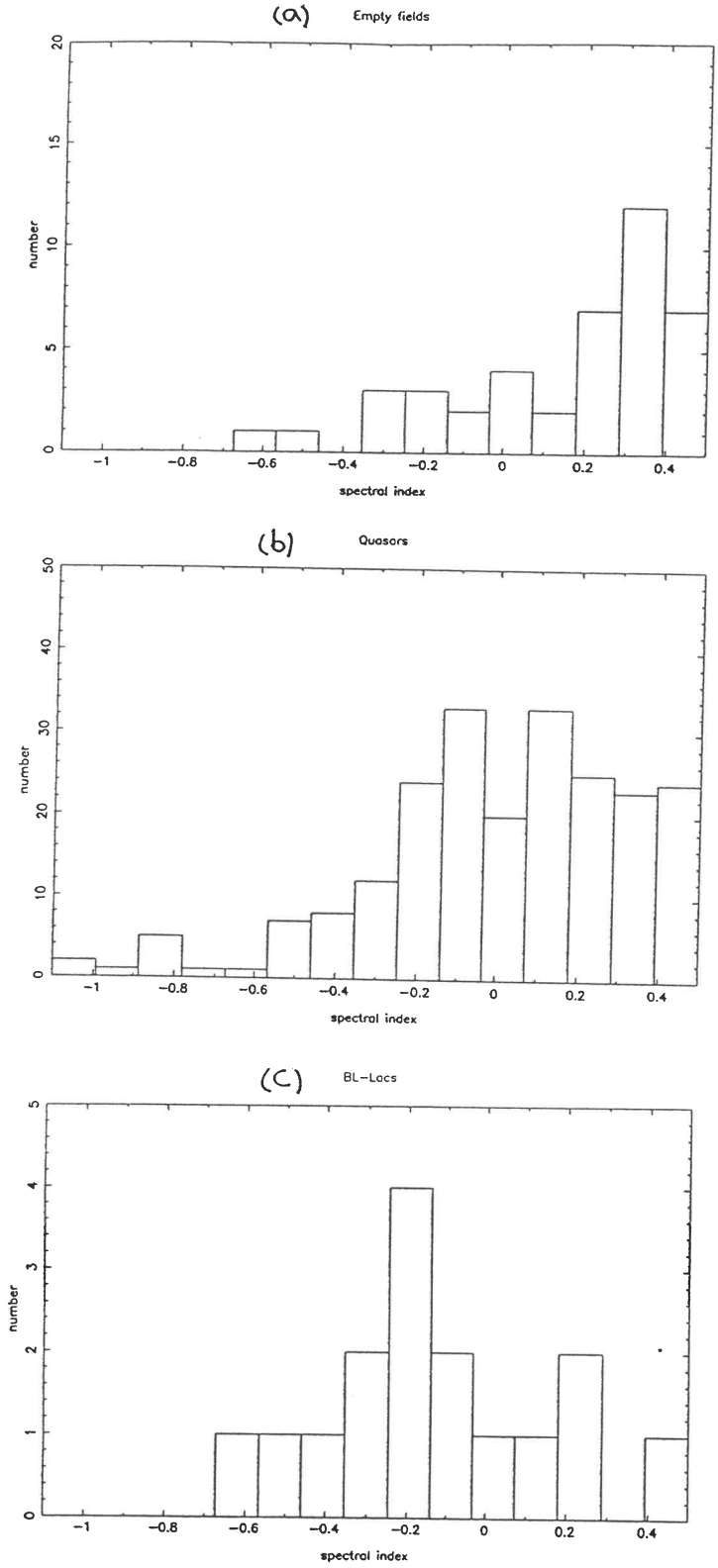

Figure 23: Flat spectrum sample from the Parkes catalogue showing distributions in spectral indices for (a)Empty fields, (b)Quasars, (c)BL-Lacs.

6.6 Suggested Further Work.

In this section, further work that may aid in determining the nature of the empty fields and their possible use in estimating the true amount of absorption by dust towards quasars will be discussed.

An initial question we may ask is how many of the empty fields are associated with high redshift quasars with $z > 2$? If empty fields represent members of the high redshift quasar population, then will the fall off in quasar numbers be less than that observed for optical quasars? This may be investigated through large faint optical quasar surveys that may also yield a substantial number of empty fields. Identifications may then be followed up by infrared spectroscopy for the determination of redshifts. Near IR spectroscopy would be prefered where it may be possible from low resolution spectra to identify the redshifted emission lines H$\beta(\lambda_o = 4861\text{Å})$ or H$\alpha(\lambda_o = 6562\text{Å})$. What is hoped of being acheived with infrared spectra are constraints that may be provided in high redhift quasars and empty fields that may be attributed to the presence of dust.

It would also be useful to obtain far (sub mm) IR spectra to determine to what extent it correlates with the near infrared continuum. Where is IR emission greatest? A knowledge of how the IR continuum cuts on and cuts off may give us an indication of how dust may be distributed and where it may be located. If IR spectra remain relatively steep towards longer wavelengths, then this may be the result of a redshifted strong near IR continuum.

What is the effect of dust on a qusar spectrum? Is this dependent on where the dust is located? A possible test would be to convolve a generic (composite) redshifted quasar spectrum with a dust extinction curve and comparing computed colours with those observed. A standard galactic extinction curve may be used.

It is also possible to use a "multicolour" technique that may isolate the reddening effects due to the presence of dust. Identifications in other bandpasses such as I, J, H may be used to further constrain dust properties.

If highly reddened sources are found also to be gravitationally lensed, then this will provide strong evidence that an intervening dusty mass distribution may be responsible for the obscuration. Moreover, the best test for an intervening dust hypothesis, would be to tie effects due to dust with metallic absorption line systems in quasar spectra. It may be possible to see

a correlation between the IR properties of dust (such as slopes) and strengths of metal line absorption systems associated with intervening dusty galaxies. In particular, such a test may be carried out with MgII, CIV, CO or Si systems. With the availability of significantly reddened quasar samples including empty fields, it may now be ideal to constrain dust properties with metal line absorption-a test similar to that carried out by Fall & Pei (1992) using the damped Ly-α systems.

If further quasar surveys detect a significant number of reddened, high redshift sources, then such samples may be used to determine whether there is more colour evolution than can be accounted for using our predicted colour vs z curves alone. Will there be a significant scatter in optical-IR colour towards higher redshifts that may be attributed to varying amounts of dust? Together with the metalic absorption line systems, this may give us an indication of how such dust may be distributed-uniformly or within the disks of intervening galaxies.

7 Future Prospects

As a follow up from this work, we propose to further obtain observational data from the complete sample of Savage et al. and carry out an analysis using some of the suggestions presented in the previous section. The following outline is proposed.

- Obtain images of all remaining empty fields and unidentified sources in the Savage et al. sample preferably in the bandpasses R, I, J, H and K.

- Undertake a multicolor analysis using successful identifications in the various bandpasses.

- Perform IR spectroscopy in the K-band for possible redshift determination of optically obscured sources.

- Tie reddening due to dust obscuration with metal line absorbtion systems from analysing infrared spectra.

- Model effects due to dust using galactic extinction curves to represent the properties of the intervening medium.

- Follow up and analyse available X-ray data.

- Generally determine an upper limit on the true amount of dust associated with the reddening observed in various sources and attempt to strengthen the unified models for AGN.

8 Conclusion

I have presented in this project, 11 optical empty fields which were selected from a complete sample of flat spectrum radio sources. Ten of these sources have been succesfully identified in the infrared and more than half of them have resulted in an exceedingly reddened optical-infrared colour as compared with that of a previously optically selected quasar sample.

It is suggested that obscuration due to dust is present and that high redshift quasars may be significantly obscured at optical wavelengths due to either dust in intervening galaxies, associated with the quasar itself, or a combination of both.

The main aim is to determine the true amount of dust which may offer a simple explanation for why we do not see large enough numbers of high redshift quasars. If such a theory is correct, we may see evidence for dust in the infrared spectra of quasars or associated with metal line absorption systems. Overall, if surveys discover a substantial number of optically faint and reddened high redshift quasars, then we should expect that they will also show a significant number of optical-empty field sources. These will be good candidates to test the dust hypothesis. This work has substantial room for expansion and may further increase our understanding of the properties of quasars and the intervening medium.

Acknowledgments

I would like to thank Paul Francis and Jonathan McDowell who have allowed me to use their composite quasar spectra as well as Ann Kinney for gratefully providing me with valuable hints and suggestions. I thank Brett Holman for the helpful computing tips and thankyou to my supervisor Rachel Webster, who has provided the observational data as well as for lots of encouragement and many helpful comments.

References

Angel, J.R.P. & Stockman, H.S. 1980, *Ann.Rev.Astron. & Astrophys.*, **18**, 321.

Antonucci, R. 1993, *Ann.Rev.Astron. & Astrophys.*, (Univ. of California preprint).

Barvainis, R. 1987, *Ap.J.*, **350**, 537.

Barvainis, R. 1992, *in Maryland Conf. proceedings No.254.*, p.129.

Begelman, M.C. *et al.* 1984, *Rev.Mod.Phys.*, **56**, 255.

Begelman, M.C. 1985, *in Astrophysics of Active Galaxies and Quasi-stellar Objects*, ed. J.S. Miller, (Mill Valley CA) p.411.

Blandford, R.D. 1990, *SAAS-Free Advanced Course 20: Active Galactic Nuclei*, (Springer Verlag).

Blandford, R.D. & Rees, M.J. 1978, *in Pittsburgh Conference on BL-LAC objects*, p.328.

Bolton, J.G. *et al.* 1979, *Aust.J.Phys.Astrophys.Suppl.No. 46.*

Boyle, B.J. 1992, *in Proc. Texas-ESO/CERN Conf. on relativistic Astrophysics.*

Boyle, B.J. *et al.* 1988, *Mon.Not.R.Astron.Soc.*, **235**, 935.

Braccesi, A. 1983, *in Early Evolution of the Universe and its Present Structure, IAU Symp.No.104*, p.23.

Burbidge, G. *et al.* 1990, *Ap.J.Suppl.*, **74**, 675.

Caganoff, S. *PhD. Thesis (MSSSO)*

Cohen, M.H. *et al.* 1983, *Ap.J.*, **272**, 383.

Condon, J.J. *et al.* 1978, *Astron.J.*, **83**, 1036.

Cristiani, S. & Vio, R. 1990, *Astron. & Astrophys.*, **227**, 385.

Cutri, R.M. 1984, *Ap.J.*, **287**, 566.

Dunlop, J.S. *et al.* 1989, *Mon.Not.R.Astron.Soc.*, **238**, 1171.

Edelson, R.A. & Malkan, M. 1987, *Ap.J.*, **323**, 516.

Elvis M. *et al.* 1993, *CFA preprint No. 3692*

Fall, S.M. & Pei, Y.C. 1989, *Ap.J.(Lett.)*, **341**, L5.

Fall, S.M. & Pei, Y.C. 1992, *Space Telescope Science Institute*, preprint No.677.

Filippenko, A.V. & Sargent, W.L.W. 1985, *Ap.J.Suppl.*, **57**, 503.

Foltz, C.B. *et al.* 1987, *Astron.J.*, **94**, 1423.

Foltz, C.B. *et al.* 1989, *Astron.J.*, **98**, 1959.
Francis, P. 1991, *Ph.D. thesis.*
Francis, P. *et al.* 1991, *Ap.J.*, **373**, 465.
Gehren, T. *et al.* 1984, *Ap.J.*, **278**, 11.
Green, R.F. *et al.* 1986, *Ap.J.Suppl.*, **61**, 305.
Gunn, J.E. 1979, *in Active Galactic Nuclei*, ed. C. Harzard, (Cambridge University Press), p.213.
Harzard, C. *et al.* 1963, *Nature*, **197**, 1037.
Heisler, J. & Ostriker, J.P. 1988, *Ap.J.*, **332**, 543.
Hewitt, J.N. *et al.* 1993, *Astron.J.*, (MIT preprint).
Huchra, J.P. 1977, *Ap.J.*, **217**, 928.
Impey, C.D. 1992, *in Energy Distributions of AGN, Steward Observatory Preprint No. 1090.*
Impey, C.D. & Neugebauer, G. 1988, *Astron.J.*, **95**, 307.
Jones, T.W. *et al.* 1974, *Ap.J.*, **192**, 261.
Kardashev, N.S. *et al.* 1985, *in Quasars, IAU Symp.No.119*, p.383.
Koo, D.C. & Kron, R.G. 1982, *Astron. & Astrophys.*, **105**, 107.
Maccacaro, T. *et al.* 1984, *Ap.J.(Lett.)*, **284**, L23.
Malkan, M.A. 1983, *Ap.J.*, **268**, 582.
Malkan, M.A. *et al.* 1984, *Ap.J.*, **280**, 66.
Malkan, M.A. 1989, *in Theory of Accretion Disks*, ed. F.Meyer *et al.*, (Kluwer Academic Publishers).
Marshall, H.L. 1985, *Ap.J.*, **299**, 109.
Matthews, T.A. & Sandage, A.R. 1963, *Ap.J.*, **138**, 30.
McAlary, C.W. & Rieke, G.H. 1988, *Ap.J.*, **333**, 1.
McKee, C.F. & Petrosian, V. 1974, *Ap.J.*, **189**, 17.
Mihalas, D. & Binney, J. 1981, *Galactic Astronomy,* 2^{nd} *ed.Freeman.*
Neugebauer, G. *et al.* 1979, *Ap.J.*, **230**, 79.
Ostriker, J.P. & Cowie, L.L. 1981, *Ap.J.(Lett.)*, **243**, L127.
Ostriker, J.P. & Heisler, J. 1984, *Ap.J.*, **278**, 1.
Owen, F.N. 1985, *in Quasars, IAU Symp.No.119*, p.173.
Peacock, J.A. & Dunlop, J.S. 1985, *in Quasars, IAU Symp.No.119*, p.455.
Peacock, J.A. 1985, *Mon.Not.R.Astron.Soc.*, **217**, 601.
Perry, J.J. 1985, *in Quasars, IAU Symp.No.119*, p.307.
Peterson, B.A. 1985, *in Quasars, IAU Symp.No.119*, p.555.
Rees, M.J. 1969, *Nature*, **278**, 788.
Rees, M.J. 1985, *in Quasars, IAU Symp.No.119*, p.3.

Rees, M.J. 1984, *Ann.Rev.Astron. & Astrophys.*, **22**, 471.
Rieke, G.H. *et al.* 1979, *Ap.J.(Lett.)*, **232**, L151.
Rieke, G.H. *et al.* 1982, *Ap.J.*, **263**, 73.
Ryle, M. & Scheuer, P.A.G. 1935, *Proc.Roy.Soc.A.*, **230**, 448.
Ryle, M. & Sandage, A.R. 1964, *Ap.J.*, **139**, 419.
Sanders, D.B. *et al.* 1989, *Ap.J.*, **347**, 29.
Savage, A. *et al.* 1990, *Aust.J.Phys.*, **43**, 241.
Schmidt, M. 1965, *Ap.J.*, **141**, 1295.
Schmidt, M. 1968, *Ap.J.*, **151**, 393.
Schmidt, M. & Green, R.F. 1983, *Ap.J.*, **269**, 352.
Schmidt, M. 1989, *in Highlights of Astronomy.*, vol.8, ed. D. McNally, (Kluwer), p.33.
Schneider, D.P. *et al.* 1991b, *Astron.J.*, **102**, 837.
Smith, M.G. 1981, *in Investigating the Universe*, ed. F.D. Kahn, p.151.
Terlevich, R. & Melnick, J. 1985, *Mon.Not.R.Astron.Soc.*, **213**, 841.
Valtaoja, E. 1985, *in Quasars, IAU Symp.No.119*, p.79.
Véron, P. 1983, *in Quasars and Gravitational Lenses.*, ed. J.P. Swings, (Inst. d'Astrophysique, Liege), p.210.
Warren, S.J. & Hewitt, P.C. 1990, *Rep.Prog.Phys.*, **53**, 1095.
Weedman, D.W. 1986, *Quasar Astronomy.*, (Cambridge University Press).
Wolfe, A.M. *et al.* 1986, *Ap.J.Suppl.*, **61**, 249.
Young, P. *et al.* 1980, *Ap.J.*, **241**, 507.
Zombeck, M.V. 1982, *in Handbook of Space Astronomy and Astrophysics.* (Cambridge Univ. Press), p.58.